https://doi.org/10.5194/acp-2020-1263
Preprint. Discussion started: 22 December 2020

Atmospheric Chemistry and Physics Discussions

Time dependent source apportionment of submicron organic aerosol for a rural site in an alpine valley using a rolling PMF window

Gang Chen[1*], Yulia Sosedova[1*], Francesco Canonaco[1,2], Roman Fröhlich[1], Anna Tobler[1,2], Athanasia Vlachou[1], Kaspar R. Daellenbach[1], Carlo Bozzetti[2], Christoph Hueglin[3], Peter Graf[3], Urs Baltensperger[1], Jay G. Slowik[1], Imad El Haddad[1], and André S.H. Prévôt[1**]

[1]Laboratory of Atmospheric Chemistry, Paul Scherrer Institute, CH-5232 Villigen PSI, Switzerland

[2]Datalystica Ltd., Park innovAARE, CH-5234 Villigen, Switzerland

[3]Empa, Swiss Federal Laboratories for Materials Science and Technology, Laboratory for Air Pollution and Environmental Technology, CH-8600 Dübendorf, Switzerland

** G.C. and Y.S. contributed equally to this manuscript*

*** Correspondence to:* André S. H. Prévôt (andre.prevot@psi.ch)

https://doi.org/10.5194/acp-2020-1263
Preprint. Discussion started: 22 December 2020

Atmospheric Chemistry and Physics Discussions

Abstract

We have collected one year of aerosol chemical speciation monitor (ACSM) data in Magadino, a village located in the south of the Swiss Alpine region, which is one of the most polluted areas in Switzerland. We analysed the mass spectra of organic aerosol (OA) by positive matrix factorization (PMF) using Source Finder Professional (SoFi Pro) to retrieve the origins of OA. Therein, we deployed the rolling algorithm to account for the temporal changes of the source profiles, which is closer to the real world. As the first ever application of rolling PMF analysis for a rural cite, we resolved two primary OA factors (traffic-related hydrocarbon-like OA (HOA) and biomass burning OA (BBOA)), one local OA (LOA) factor, a less oxidized oxygenated OA (LO-OOA) factor, and a more oxidized oxygenated OA (MO-OOA) factor. HOA showed stable contributions to the total OA through the whole year ranging from 8.1–10.1%, while the contribution of BBOA showed a clear seasonal variation with a range of 8.3–27.4% (highest during winter, lowest during summer) and a yearly average of 17.1%. The OOA was represented by two factors (LO-OOA and MO-OOA) throughout the year. OOA contributed 71.6% of the OA mass, varying from 62.5% (in winter) to 78% (in spring and summer). The uncertainties (σ) for the modelled OA factors (i.e., rotational uncertainty and statistical variability of the sources) varied from ±4% (LOA) to a maximum of ± 40% (LO-OOA). Considering the fact that BBOA and LO-OOA (showing influences of biomass burning in winter) had significant contributions to the total OA mass, we suggest a reduction and control of the residential heating as a mitigation strategy for better air quality and lower PM levels in this region. In Appendix A, we conducted a head-to-head comparison between the conventional seasonal PMF analysis and the rolling mechanism. It showed similar or slightly improved results in terms of mass concentrations, correlations with external tracers and factor profiles of the constrained POA factors. The rolling results show smaller scaled residuals and enhanced correlations between OOA factors and corresponding inorganic salts than those of the seasonal

https://doi.org/10.5194/acp-2020-1263
Preprint. Discussion started: 22 December 2020

Atmospheric Chemistry and Physics Discussions

solutions, was most likely because the rolling PMF analysis can capture the temporal variations of the oxidation processes for OOA sources. Specifically, the time dependent factor profiles of MO-OOA and LO-OOA can well explain the temporal viabilities of two main ions for OOA factors, *m/z* 44 (CO_2^+) and *m/z* 43 (mostly $C_2H_3O^+$). This rolling PMF analysis therefore provides a more realistic source apportionment (SA) solution, with time-dependent OA sources. The rolling results show also good agreement with offline Aerodyne aerosol mass spectrometer (AMS) SA results from filter samples, except for winter. This is likely because the online measurement is capable of capturing the fast oxidation processes of biomass burning sources. This study demonstrates the strengths of the rolling mechanism and provides a comprehensive criterion list for ACSM users to obtain reproducible SA results and is a role model for similar analyses of such world-wide available data.

1 Introduction

Atmospheric particulate matter (PM) affects human health and climate. In particular, it influences the radiative balance (IPCC, 2014; von Schneidemesser et al., 2015), reduces visibility (Chow et al., 2002; Horvath, 1993), and negatively affects human health by triggering respiratory and cardiovascular diseases and allergies (Daellenbach et al., 2020; Dockery and Pope, 1994; Mauderly and Chow, 2008; Monn, 2001; Pope and Dockery, 2006; von Schneidemesser et al., 2015). Fine PM exposure strongly correlates with the global mortality rate. Lelieveld et al. (2015) estimated that outdoor air pollution, mostly $PM_{2.5}$ (PM with an aerodynamic diameter smaller than 2.5 µm) causes 3.3 million premature deaths per year worldwide. Despite of this correlation, different aerosol sources may have strongly different effects on health (Daellenbach et al., 2020). Thus, both climate and health effects are affected by particle chemical composition, which is related to emission sources of primary particles and

https://doi.org/10.5194/acp-2020-1263
Preprint. Discussion started: 22 December 2020


Atmospheric Chemistry and Physics Discussions

precursor gases for secondary aerosol (IPCC, 2014; Jacobson et al., 2000; Jacobson, 2001; Lelieveld et al., 2015; Ramanathan et al., 2005).

Organic aerosol (OA) constitutes 20–90% fine PM (Jimenez et al., 2009; Murphy et al., 2006; Zhang et al., 2007), and contains millions of chemical compounds. Since OA is subject of an extremely complex mixture of chemical constituents, with highly dynamic spatial and temporal (seasonal, diurnal, etc.) variability of directly emitted particles and gas-phase precursors and a complex chemical processing in the atmosphere, elucidation of the chemical composition and physical properties of OA remains challenging. Identification and quantification of OA sources with a sophisticated interpolation of both spatial and temporal variabilities are essential for a development of effective mitigation strategies for air pollution and a better assessment of the aerosol effect on both health and climate.

OA source apportionment (SA) and PM composition has been studied extensively using the Aerodyne aerosol mass spectrometer (AMS) (Canagaratna et al., 2007). However, due to the complexity of the AMS measurements and their high operational expenses, AMS campaigns are often limited to short time periods of a few weeks to months. The aerosol chemical speciation monitor (ACSM) allows for unattended long-term observation (>1 year) of non-refractory aerosol particles (Ng et al., 2011a; Fröhlich et al., 2013). It makes it possible to investigate also the long-term temporal variations of OA sources, which is crucial for policymakers to introduce or validate aerosol-related environmental policies.

Positive matrix factorization (PMF) has been used in various studies for SA of OA (Aiken et al., 2009; Hildebrandt et al., 2011; Lanz et al., 2007; Mohr et al., 2012; Schurman et al., 2015; Zhang et al., 2011). The multilinear engine (ME-2) implementation of PMF (Paatero, 1999) improves model performance by allowing the use of *a priori* information (constraints on source profiles and/or time series) to direct the model towards environmentally meaningful solutions

https://doi.org/10.5194/acp-2020-1263
Preprint. Discussion started: 22 December 2020


Atmospheric Chemistry and Physics Discussions

(Canonaco et al., 2013; Crippa et al., 2014; Fröhlich et al., 2015; Lanz et al., 2008; Ripoll et al., 2015). For long-term data (one year or more) with high time resolution, the composition of a given source could change considerably due to the meteorological and seasonal variabilities. However, a major limitation of PMF is the assumption of static factor profiles, such that it fails to respond to these temporal changes. Therefore, long-term chemically speciated data have been evaluated monthly or seasonally (Bressi et al., 2016; Canonaco et al., 2015; Minguillón et al., 2015; Petit et al., 2014; Reyes-Villegas et al., 2016; Ripoll et al., 2015) to at least take the seasonal variations into account. To improve analysis of long-term ACSM datasets, a novel approach that utilizes PMF analysis on a smaller time rolling window was first proposed by Parworth et al. (2015) and further refined using ME-2 by Canonaco et al. (2020). The short length of the rolling PMF window allows the PMF model to take the temporal variations of the source profiles into account (e.g., biogenic versus domestic burning influences on oxygenated organic aerosol (OOA)), which normally provides a better separation between OA factors. In addition, using this technique together with bootstrap resampling and a random *a*-value approach allows users to assess the statistical and rotational uncertainties of the PMF results (Canonaco et al., 2020; Tobler et al., 2020).

In this work, we conducted a one year ACSM measurement from September 2013 to October 2014 in Magadino, located in an alpine valley in southern Switzerland. We present a comprehensive analysis of the ACSM dataset measured in Magadino using a novel PMF technique, the “rolling PMF”. In addition, we also compare the results of the rolling PMF with the source apportionment of offline AMS filter samples (Vlachou et al., 2018) and conventional seasonal PMF analysis.

https://doi.org/10.5194/acp-2020-1263
Preprint. Discussion started: 22 December 2020

Atmospheric Chemistry and Physics Discussions

2 Methodology

2.1 Sampling site

Magadino is in a Swiss alpine valley (46°90'37'' N, 85°60'2'' E, 204 m.a.s.l.), where the sampling site located. This site belongs to the Swiss National Air Pollution Monitoring Network (NABEL, https://www.empa.ch/web/s503/nabel). It is around 1.4 km away from the local train station, Cadenazzo, around 7 km away from the Locarno Airport, and nearly 8 km away from the Lake Maggiore. This station is surrounded by agricultural fields within a rural area, which is considered as a rural background site. It can be potentially affected by domestic wood burning, adjacent agricultural activity and transit traffic through the valley. The site topography favours quite high PM levels due to stagnant meteorological conditions or boundary layer inversions, especially in winter. The annual average PM_{10} concentration in Magadino exceeded the annual average PM_{10} limit value for Switzerland (20 $\mu g \cdot m^{-3}$) for five years out of the period 2007–2016 (Meteotest, 2017; The Swiss Federal Council, 2018).

2.2 ACSM measurements

In this study, chemical composition and mass loadings of non-refractory constituents of ambient submicron aerosol particles (NR-PM_1) were measured by an Aerodyne quadrupole ACSM (Ng et al., 2011a). The ACSM uses the same sampling and detection technology as the AMS but is simplified and designated for long-term monitoring applications by reducing maintenance frequency, at the cost of lower sensitivity, restriction to integer mass resolution, and no size measurement. Same as for the AMS, sampled submicron particles enter the instrument through a critical orifice (100 µm I.D.) at a flow rate of 1.4 $cm^3\ s^{-1}$ (at 20 °C and 1 atm). The sampling flow will pass either through a particle filter or directly into the system using an automated 3-way switching valve, that is switched every ~30 s. The sampled particles are focused by an aerodynamic lens into a narrow beam and impact on a tungsten surface of around 600 °C, where the non-refractory particles vaporize and are subsequently ionized by an

https://doi.org/10.5194/acp-2020-1263
Preprint. Discussion started: 22 December 2020

Atmospheric Chemistry and Physics Discussions

electron impact source (70 eV). The resulting ions are detected by a quadrupole mass-spectrometer up to a mass to charge ratio *m/z* = 148 Th. The particle mass spectrum is represented by the difference of the total ambient air signal and the particle-free signal.

The quantification of ACSM data requires an estimation of the fraction of NR-PM_1 that bounces off the oven without being vaporized and therefore is not detected (Canagaratna et al., 2007; Matthew et al., 2008). A collection efficiency (CE) factor is typically introduced to correct for particle bounce, which depends on the particulate water content (Matthew et al., 2008), ammonium nitrate mass fraction (ANMF) and acidity (Middlebrook et al., 2012). To eliminate humidity effects on CE, a Nafion membrane dryer (Perma Pure MD) was installed on the sampling inlet. In this study, we compared both, a constant CE of 0.45 and a time-dependent CE correction suggested by Middlebrook et al., (2012). It showed that data corrected with a constant CE had a better correlation and slope closer to 1 when comparing with the chromatographic SO_4^{2-}, NO_3^-, and Cl^- anions (Fig. S1a). In addition, as more than 93.5% data have an ANMF smaller than 0.4, only 6.5% of data would be impacted by a time-dependent CE correction, therefore, the ammonium nitrate particles doesn't have significant effects on CE for this dataset. Overall, this dataset agrees with external TEOM measurement of both $PM_{2.5}$ and PM_{10} daily mass concentrations as shown in Fig S1c with a constant CE value.

The ACSM filament burnt out on 14 April, 2014. This was addressed by switching to the backup filament already installed within the instrument (no venting required). Calibration of the relative ionization efficiencies (RIE) of particulate nitrate, sulphate, and ammonium was conducted using size-selected (300 nm) pure NH_4NO_3 and pure $(NH_4)_2SO_4$ particles. Calibrations of the relative ionisation efficiency (RIE), *m/z* scale, and the sampling flow was performed every 2 months. In this study, we used the averaged RIEs for nitrate, sulphate, and ammonium, the exact values are shown in Fig S1.

https://doi.org/10.5194/acp-2020-1263
Preprint. Discussion started: 22 December 2020

Atmospheric Chemistry and Physics Discussions

2.3 Complementary measurements

Meteorological data, including temperature, precipitation, wind speed, wind direction, and solar radiation are monitored at the NABEL station. In addition, concentrations of trace gases (SO_2, O_3, NO_x), equivalent black carbon (eBC), and PM_{10} were measured with a time resolution of 10 minutes. We used an aethalometer (AE 31 model by Magee Scientific Inc.) to measure eBC concentrations. Therefore, we conducted SA of eBC by following Zotter et al. (2017) using Ångstrom exponents for eBC from traffic $\alpha_{tr} = 0.9$ and wood burning $\alpha_{wb} = 1.68$. More details about eBC source apportionment are provided in Section 1 of the SI.

2.4 Preparation of the data and error matrices for PMF

In this study, we used acsm_local_1610 software (Aerodyne Research Inc.) to prepare the PMF input matrix. In total, this dataset includes 19'708 time points and 67 ions. Of these, CO_2^+-related variables (I_{O+} (m/z = 16), I_{HO+} (m/z = 17), and I_{H2O+} (m/z = 18)) were excluded from the spectral matrix prior to a PMF analysis. They are reinserted into the OA factor mass spectra after the PMF analysis using the ratio from the fragmentation table (Allan et al., 2004); the factor concentrations are likewise adjusted. The measurement error matrix was calculated according to Allan et al. (2003, 2004), with a minimum error considered for the uncertainty of all variables in the data matrix as in Ulbrich et al. (2009). Following the recommendations in Paatero and Hopke (2003) and Ulbrich et al. (2009), the measurement uncertainty for variables (m/z) with a signal-to-noise ratio (S/N) < 2 (weak variables) and S/N < 0.2 (bad variables) were increased by a factor of 2 and 10, respectively. In total, 27 weak ACSM variables were down-weighted. Additionally, m/z 12 and 13 were not considered during the PMF analyses, due to being noisy and their overall negative signal. Moreover, m/z 15 is not only very noisy (S/N = 0.09), but may be also affected by high biases due to potential interference with air signals.

https://doi.org/10.5194/acp-2020-1263
Preprint. Discussion started: 22 December 2020

Atmospheric Chemistry and Physics Discussions

2.5 Factor analysis of the organic mass spectra

PMF has been demonstrated to be a useful tool to retrieve the sources of measured organic aerosol mass spectra with a bilinear factor model (Paatero and Tapper, 1994; Ulbrich et al., 2009):

$$x_{ij} = \sum_{k=1}^{p} g_{ik} \times f_{kj} + e_{ij} \quad (1)$$

where x_{ij} is the mass concentration of the j^{th} mass spectral variable in the time point i^{th}; g_{ik} is the contribution of the k^{th} factor in the i^{th} time point; f_{kj} is the concentration of the j^{th} mass spectral variable in the k^{th} factor; and e_{ij} is the residual of j^{th} variable of the mass spectra in i^{th} time point. The superscript, p represents the number of factors, which is determined by the user. The cost function of PMF uses least squares algorithm by iteratively minimizing the following quantity Q:

$$Q = \sum_{i=1}^{n} \sum_{j=1}^{m} \left(\frac{e_{ij}}{\sigma_{ij}}\right)^2 \quad (2)$$

where σ_{ij} is an element in the $n \times m$ matrix of the measurement uncertainties, which corresponds point-by-point to x_{ij}. In addition, we normalized quantity $\frac{Q}{Q_{exp}}$ as a mathematical metric during PMF analysis, where the Q_{exp} is:

https://doi.org/10.5194/acp-2020-1263
Preprint. Discussion started: 22 December 2020

Atmospheric Chemistry and Physics Discussions

$$Q_{\exp} = (n \times m) - p \times (n + m) \quad (3)$$

199

200 The $\frac{Q}{Q_{exp}}$ supports the user to determine the number of factors required for the model by
201 investigating the effects on this quantity of adding/removing a factor. However, PMF itself
202 suffers from rotational ambiguity because of the fact that the object function, Q does not
203 provide unique solutions, that is when $\mathbf{G} \cdot \mathbf{F} = \mathbf{G} \cdot \mathbf{T} \cdot \mathbf{T^{-1}} \cdot \mathbf{F}$, PMF provides a similar value of
204 Q but very different solutions (rotated matrix $\bar{\mathbf{G}} = \mathbf{G} \cdot \mathbf{T}$ (rotated factor time series) and $\bar{\mathbf{F}} =$
205 $\mathbf{T^{-1}} \cdot \mathbf{F}$ (rotated factor profiles)). Only one of or even none of these rotated solutions may be
206 atmospherically relevant. The ME-2 solver (Paatero, 1999) enables theoretically full rotational
207 control over the factor solutions, which is implanted here by imposing constraints via the *a*-
208 value approach on one or more elements of **F** and/or **G** (Paatero and Hopke, 2009). The *a*-value
209 (ranging from 0 to 1) determines how much the resulting factor ($f_{j,solution}$) or time series
210 ($g_{j,solution}$) can vary from the input reference factor ($f_{j,reference}$) or time series ($g_{j,reference}$)
211 as shown in Eq. 4a and 4b:

212

$$f_{j,solution} = f_{j,reference} \pm a \cdot f_{j,reference} \quad (4a)$$

$$g_{j,solution} = g_{j,reference} \pm a \cdot g_{j,reference} \quad (4b)$$

213

214 Previous work using *a*-values has shown to efficiently retrieve environmentally reasonable
215 PMF solutions. This is due to the presence of legitimate *a priori* constraints which decrease the
216 degree of rotational ambiguity (Canonaco et al., 2013, 2020; Crippa et al., 2014; Lanz et al.,
217 2008). Here we configured the ME-2 solver and analysed PMF results using SoFi (Source

https://doi.org/10.5194/acp-2020-1263
Preprint. Discussion started: 22 December 2020


Atmospheric Chemistry and Physics Discussions

Finder, Datalystica Ltd., Villigen, Switzerland) Pro 6.D interface (Canonaco et al., 2013, 2020), developed within the IGOR Pro software (WaveMetrics Inc., Lake Oswego, OR, USA).

Running PMF over the long-term ACSM datasets assumes that the OA source profiles are static within this time window. This can lead to large errors, since OA chemical fingerprints are expected to vary over time (Paatero et al., 2014). For example, Canonaco et al. (2015) showed that the variability of summer and winter OOA cannot be accurately represented by a single pair of OOA profiles. A common way to reduce the model uncertainty arising from this source is to choose a proper number of OA factors (Sug Park et al., 2000), and then perform a PMF analysis on a subset of measurements to capture temporal features of OA chemical fingerprints. Such characterization of OA sources on a seasonal basis has been demonstrated in a number of studies (Crippa et al., 2014; Lanz et al., 2008; Minguillón et al., 2015; Petit et al., 2014; Ripoll et al., 2015; Zhang et al., 2019).

2.6 Rolling PMF analysis with ME-2

In this study, we performed PMF runs with *a priori* constraints (factor profiles) retrieved from seasonal bootstrap analysis (Section 2.2 in the SI) on a small and rolling window (i.e., 1, 7, 14, and 28 days) that could move across the entire dataset with a step of one day (Canonaco et al., 2020; Parworth et al., 2015). In addition, we used the bootstrap re-sampling strategy, which can randomly choose a subset of the original matrix and replicate some of the rows/columns to create a new same-size matrix (Efron, 1979). Here, we combined this rolling PMF analysis with the bootstrap strategy and random *a*-values for constrained factor profiles to estimate the statistical and rotational uncertainties of this PMF analysis. More details of this novel technique is found in Canonaco et al. (2020).

https://doi.org/10.5194/acp-2020-1263
Preprint. Discussion started: 22 December 2020

2.6.1 Window settings

In order to retrieve appropriate constraints, we performed PMF *pre-tests* and bootstrap analysis for different seasons. More details of the steps, settings of these analysis can be found in Section 2 of the SI. Here, we constrained primary OA factor profiles (hydrocarbon-like OA factor (HOA) and biomass burning OA (BBOA)) as well as the factor profile of a local factor (LOA) using the *a*-value technique in the rolling PMF analysis. The reference profiles of HOA and BBOA were from the winter bootstrapped PMF solution (Dec, Jan, and Feb) as shown in Fig. S6. With a higher contribution of the biomass burning trace ion *m/z* 60 in the winter, we expect a more representative and robust BBOA profile from the winter solution than from other seasons. The LOA profile was retrieved from the summer bootstrapped PMF solution (Jun, Jul, and Aug) (Fig. S6). To allow the factor profile to adapt itself over time, a random *a*-value within a range of 0.4 with a step of 0.1 is applied for HOA and BBOA. Canonaco et al. (2020) suggested that an upper *a*-value of 0.4 is sufficient to cover the temporal variation of OA source profiles. Moreover, due to the uniqueness of the LOA chemical profile, it is tightly constrained with a constant *a*-value of 0.05. The LOA factor appeared only after the filament had been changed (14 April, 2014), and its mass spectrum is dominated by nitrogen-containing fragments (at *m/z* 58, 84, and 98). The instrument setup thus influenced strongly the sensitivity of these components (likely due to influences of surface ionization). Therefore, this factor was considered in the PMF analysis, but no further interpretation of its potential source will be covered in this manuscript.

In total, we constrained HOA and BBOA factors with random *a*-value (0–0.4, with a step of 0.1), and an exact *a*-value (0.05) for LOA factor in the rolling PMF analysis. There are 25 (N=5×5) possible *a*-value combinations within an individual rolling window. Therefore, 50 PMF iterations for each time window are sufficient to cover all possibilities of the *a*-value combinations. With the rolling window of 50 repeats, each data point (except the data within

https://doi.org/10.5194/acp-2020-1263
Preprint. Discussion started: 22 December 2020

Atmospheric Chemistry and Physics Discussions

the first and last time window) will actually have many PMF iterations (i.e., *N*=length of the window×50), where bootstrap resampling and random combinations of constraints is performed. This allows to estimate the statistical and rotational uncertainties of the PMF factors (Canonaco et al., 2020). To find the optimum length of the time windows, we tested four different lengths of the time windows (N=1, 7, 14, 28) using the same approaches as in Canonaco et al. (2020). We determined the optimum length of the time window based on the number of missing data points (un-modelled data due to the selection based on the criteria) while applying the same thresholds for the same criteria.

2.6.2 Criteria settings

Performing a rolling analysis for a one-year data with 50 repeats per window requires several tens of thousands of PMF runs. Manual inspection of all PMF runs is impractical and therefore was replaced by monitoring user-defined criterion scores (Canonaco et al., 2020). In this study, R^2 values of the time series of modelled HOA vs NO_x and eBC_{tr} were used for HOA. The BBOA factor was inspected using the variation of *m/z*=60 explained by BBOA (Table S1). For these time series based criteria, (criterion 1 to criterion 3 in Table S1), we deployed student t-test to minimize subjective judgment while determining the thresholds (more discussions in Section 2.3 of the SI).

Typically, OOA factors are dominated by the signals of f_{43} ($C_2H_3O^+$ at *m/z* = 43) and f_{44} (CO_2^+ at *m/z* = 44) that correspond to the less and more oxygenated ion fragments (Canonaco et al., 2015; Ng et al., 2010), where *f* is the fraction of a variable, *i.e.* the intensity $I_{m/z}$ normalized by the sum of the intensities of all organic *m/z* variables. In this study, we were able to retrieve two OOA factors (i.e., more oxidized OOA (MO-OOA) and less oxidized OOA (LO-OOA)) for the whole year, while MO-OOA can be at either at 4th or 5th position because there are two unconstrained factors. Thus, we used the f_{44} for the 4th factor to sort the unconstrained OOA

https://doi.org/10.5194/acp-2020-1263
Preprint. Discussion started: 22 December 2020

Atmospheric Chemistry and Physics Discussions

factors to ensure MO-OOA and LO-OOA sitting on the 4th and 5th position, respectively. The details of the sorting scheme can be found in Canonaco et al. (2020). At the same time, we also monitored the f_{43} in LO-OOA and f_{44} in MO-OOA to make sure they are not zero. With this set of criteria, we were able to only select "good" (atmospherically relevant) PMF runs before averaging.

3 Results and discussion

3.1 Overview of PM_1 sources in Magadino

Considering that the major part of eBC is within PM_1 (Schwarz et al., 2013), we added eBC to the total NR-PM_1 from the ACSM to perform a mass closure analysis with $PM_{2.5}$/PM_{10} from filters. The gravimetric $PM_{2.5}$ and PM_{10} show a high correlation with total estimated PM_1 (NR-PM_1 +eBC) (Fig. S1c). The slopes of the linear fits (± 1 standard deviation) are 1.62 ± 0.05 (R^2 = 0.81, N=79) for $PM_{2.5}$ *vs.* PM_1 and 1.84 ± 0.03 (R^2 = 0.67, N=335) for PM_{10} *vs.* PM_1. This means that the estimated PM_1 comprised 62% and 54% of the $PM_{2.5}$ and PM_{10} mass, respectively. The daily averages of the inorganic species concentrations measured by the ACSM and those measured on the filters by chromatography show a high correlation, with R^2 = 0.83 for SO_4^{2-}, R^2 = 0.82 for NO_3^- and R^2 = 0.50 for Cl^-, with slopes close to 1 (Fig. S1a). The 2-week average of total ammonium and total nitrate measured by offline AMS technique agree rather well with the ACSM ammonium (R^2 = 0.47) and nitrate (R^2 = 0.79), as shown in the plots in Fig. S1b. The ion balance of particulate ammonium, sulphate and nitrate measured by the ACSM showed that the measured aerosol particles were mostly neutral.

The daily average PM_1 components are shown in Fig. 1a, with the annual average PM_1 concentration (including eBC) for the period from September 2013 to October 2014 equal to 10.2 µg m^{-3}. In winter, the average PM_1 concentration was highest (13.8 µg·m^{-3}), with OA

https://doi.org/10.5194/acp-2020-1263
Preprint. Discussion started: 22 December 2020


Atmospheric Chemistry and Physics Discussions

312 contributing 54% to the total PM_1 mass. In summer, the average PM_1 mass concentration was
313 below 10 $\mu g \cdot m^{-3}$, but the relative contribution of the OA fraction increased to 62%.

314 Seasonally averaged diurnal cycles of NR-PM_1 and of eBC are displayed in Fig. 2. In this study,
315 all the data is based on local time (Central European Time). In fall, spring and summer, the
316 diurnals of these pollutants seem to be mainly affected by the development of the BLH, most
317 of the species show similar diurnal trends for these three seasons. In addition, summer has the
318 highest sulphate concentration, due to the enhanced photochemical production. In winter, air
319 pollutants accumulated during evening and night due to the thermal inversion. In general, eBC
320 and organics have higher levels due to enhanced biomass burning emissions and lower
321 boundary layer height (BLH). We observed distinct midday peaks of organics, sulphate, nitrate,
322 ammonium, chloride, and NO_x in the winter. Magadino experienced a series of windless, cold,
323 but sunny periods from December 2013 to January 2014, including such sharp peaks (Fig. S3a).
324 It is interpreted to be due to advection within the shallow boundary layer due to the fact that
325 both primary and secondary pollutants increased simultaneously. Local winds were very low
326 near the ground but likely locally and regionally induced orography influenced winds including
327 vertical diffusion processes were initiated during these times that are difficult track without
328 spatially distributed measurements. . Such phenomena were not observed during cloudy, cold,
329 and windless days (Fig. S3b) without thermally induced meteorological processes. Unlike other
330 seasons, the dilution process due to vertical mixing happened only after noon time due to strong
331 inversions during the night and late irradiation of the valley surface in winter.

332 3.2 Seasonal PMF *Pre-tests*

333 The automated rolling PMF analysis requires the knowledge of the reference profiles as well
334 as the number of factors. In this section, we present how number of factors were determined
335 based on seasonal PMF *pre-tests*. Initially, unconstrained PMF (3 to 6 factors) was performed

https://doi.org/10.5194/acp-2020-1263
Preprint. Discussion started: 22 December 2020


Atmospheric Chemistry and Physics Discussions

separately for the different seasons by following the SA guidelines provided by Crippa et al. (2014). Typically, the HOA profile is characterized by a high contribution of alkyl fragments (*e.g. m/z* =43, *m/z* =57) and the corresponding alkenyl carbo cations (*e.g. m/z* = 41, *m/z* = 55), and the factor profile is relatively consistent over time and different locations. The BBOA profile exhibits significant signals at *m/z* = 60 and *m/z* =73, which are well-known fragments, arising from fragmentation of anhydrous sugars present in biomass-related emissions (Alfarra et al., 2007). For the unconstrained PMF runs, the HOA profile is present throughout the whole year, while the BBOA profile exists for all seasons except in summer. However, as shown in Fig. S4, the measured fraction of *m/z* = 60 during summer was above the background level of biomass burning-related air masses, 0.3% ±0.06% (Aiken et al., 2009; Cubison et al., 2011; DeCarlo et al., 2008). In addition, the scaled residual at *m/z* = 60 was decreased when a BBOA factor profile was constrained. Thus, we decided to constrain the BBOA factor for all seasons to potentially capture some local events, such as agricultural and open fires in summer.

No evidence for the presence of a cooking-related OA (COA) factor was found based on the seasonal pre-analysis of the key fragments (*m/z* 55 and *m/z* 57). It shows no difference in the slope of the absolute mass concentration of *m/z* 55 vs *m/z* 57 for different hours of the day (Fig S5a), while different seasons show different slopes (Fig S5b). Therefore, a COA factor was not considered in the PMF model. Moreover, a rapid increase of the measured fraction of *m/z* = 58, 84, and 98 together with *m/z* 39 (potassium signal) was observed after a filament exchange on 14 April, 2014. It is likely that the ACSM's sensitivity towards those ions was changed by the filament exchange. Also, this LOA factor was present for spring, summer, and autumn in 2014 in unconstrained PMF runs all the time after the filament change. Therefore, we kept this factor for these three seasons.

https://doi.org/10.5194/acp-2020-1263
Preprint. Discussion started: 22 December 2020

Atmospheric Chemistry and Physics Discussions

For the factor(s) with secondary origin, PMF models with different number of factors (3–6) were tested to assess if the oxygenated OA (OOA) factor (with a high contribution of *m/z* 44 that is likely dominated by the CO_2^+ ion, derived from decomposition of carboxylic acids (Duplissy et al., 2011)) is separable without mixing with primary organic aerosol (POA) factors (Fig. S6). We conducted these tests independently for different seasons (autumn 2013, winter, spring, summer, autumn 2014).

We analysed winter data first by constraining a HOA factor profile (Crippa et al., 2013) with a tight *a*-value of 0.05. The 3-factor solution (with one OOA factor) showed similarly good agreement of HOA and BBOA with the external tracers (NO_x, eBC_{tr}, eBC_{wb}) as the 4-factor solution (with two OOA factors). However, the scaled residual of *m/z* 60 was reduced for the solution with two OOA factors. Moreover, the solution with one OOA factor was not sufficient to explain the variabilities of measured f_{44} vs f_{43} (excluding the primary organic aerosol (POA) factors). For 5- and 6-factor solutions the BBOA and LO-OOA factors started to split. Eventually, we selected the 4-factor solution (HOA, BBOA, MO-OOA, LO-OOA) as the best representation of the winter data.

After the bootstrap seasonal PMF runs of winter data (details in Section 2 of the SI), we extracted the HOA and BBOA profiles to use them as the reference factor profiles (Fig. S6) for the *pre-tests* of other seasons. For the spring, summer, and autumn seasons, 3- to 6-factor PMF solutions were modelled separately for each season by constraining the HOA (*a*-value=0.1) and BBOA (*a*-value=0.3) profiles. For the 3-factor solution, we observed an OOA factor with some signals at *m/z* 58, 84, and 98 which we could not relate to a specific source or process. Also the scaled residuals of variables showed significant levels for these three ions. When we increased the number of OA factors from 3 to 4, a factor dominated by *m/z* 58, 84, and 98 emerged, which we named local organic aerosol (LOA). However, the OOA factor still showed

https://doi.org/10.5194/acp-2020-1263
Preprint. Discussion started: 22 December 2020


Atmospheric Chemistry and Physics Discussions

slight signals at *m/z* 58, 84, and 98. An increase in the number of factors from 4 to 5 did not only result in a decrease in $\frac{Q}{Q_{exp}}$, but also in "clean" OOA factors without mixing with the LOA factor. A further increase in the number of factors did not change $\frac{Q}{Q_{exp}}$ substantially (< 1%), and the sixth factor was a mathematical split of the LOA factor with *m/z* 58 as the dominating variable. Thus, the 5-factor PMF model was chosen as the most appropriate for the spring, summer, and autumn 2014. Note that we did not add the LOA factor for the autumn season in 2013 since it appeared only after the filament exchange on 14 April, 2014. This LOA factor was included while running PMF because of the rapid drop of the $\frac{Q}{Q_{exp}}$ from 4 to 5 factors in the PMF model, but the source of this factor will not be discussed in the manuscript.

3.3 Full year rolling PMF analysis

Here we present the optimized time window size (14 days) (details of the time window optimization are given in Section 4 of the SI and Fig S10). In total, we considered 53.4% of the PMF runs (11087 out of 20750) with only 11 non-modelled data points. The results of the full-year PMF analysis of the 30-min resolved ACSM data are summarized in Fig. 3. The relative contributions of the OA factors are in addition shown in Fig. 3b. The primary traffic related HOA had very little variation (seasonal averages between 8.1 and 10.1%) throughout the year (Fig. 4). In contrast, BBOA showed a distinct yearly cycle (8.3–27.4%) with a yearly averaged contribution of 17.1%. It increased significantly (to 27.4%) in winter which is typical for Alpine valleys (Szidat et al., 2007). It means that biomass burning was the most important primary OA source during the cold season in Magadino. The eBC_{wb} showed similar trends as the BBOA factor time series during the cold seasons (Fig. 3c). The contribution of LOA remained small before the filament was changed on 14 April, 2014, which is expected because we could not retrieve this factor in seasonal unconstrained PMF runs before April 2014.

https://doi.org/10.5194/acp-2020-1263
Preprint. Discussion started: 22 December 2020


Atmospheric Chemistry and Physics Discussions

406 In this study, we retrieved two OOA factors, LO-OOA and MO-OOA. Total OOA (LO-
407 OOA+MO-OOA) contributed substantially to the total OA mass throughout the whole year
408 with an average contribution of 71.6% (Fig. 3b; Fig. 4). In general, the contribution of OOA to
409 the total OA mass did not vary distinctly over the seasons, but reached a maximum of 90.1%
410 on 12 June, 2014, the day with the highest daily average temperature (30.7 °C).

411 In this work, we did head-to-head comparisons between the bootstrap seasonal solutions and
412 the rolling PMF results (see Fig. A1, Fig. A2, Fig. A3, and Table A1 in the Appendix) in terms
413 of mass concentrations, factor profiles, scaled residuals, and correlations between time series
414 for each factor and corresponding external tracers. We found consistent factor profiles and
415 mass concentrations for the constrained factors (i.e., HOA, BBOA, and LOA), while OOA
416 factors showed quite some differences in both mass concentrations and factor profiles. Rolling
417 PMF provided slightly better correlations and smaller scaled residuals, therefore, we consider
418 rolling PMF results to be more environmentally reasonable than those of the seasonal PMF
419 (more details in Appendix A).

420 ### 3.3.1 Optimized OA factors retrieved from a rolling PMF model

421 The primary and secondary OA factors retrieved as an annual mean of all optimized PMF
422 solutions together with their diurnal cycles for all seasons are shown in Fig. 5. Seasonal
423 variations of the OOA factor profiles are demonstrated in Fig. 7 and further discussed in more
424 detail in Section 3.3.2. Note that the primary factors (HOA, BBOA, and LOA) were constrained,
425 where the LOA profile was tightly constrained with an *a*-value of 0.05 due to the uniqueness
426 of its chemical profile. Therefore, only a small variation was allowed for LOA, while the HOA
427 and BBOA model profiles varied more due to looser constraints (Fig. S8). HOA and BBOA
428 have averaged *a*-values of 0.207, and 0.195, respectively. In addition, they both had good
429 agreement with previous studies (Crippa et al., 2014; Ng et al., 2011b). The probability

https://doi.org/10.5194/acp-2020-1263
Preprint. Discussion started: 22 December 2020


Atmospheric Chemistry and Physics Discussions

distribution function (PDF) of applied *a*-values over time was also investigated (Fig. S8). Most selected runs chose *a*-values of 0.1–0.3 for HOA and BBOA. The OOA factors show larger variations in the chemical profiles because these two factors were not constrained due to the high variability of oxidation processes governing the secondary factors.

Due to extensive residential wood combustion combined with winter inversions, the concentrations of BBOA and eBC_{wb} were three times higher at night than at midday. As discussed above, during winter, all of the air pollutants, including all PMF factors peaked concurrently at 10–11 a.m. (local time) due to development of the mixed boundary layer (light blue markers in Fig. 2 for total PM_1 and Fig. 5b). In summer, an additional local photochemical production led to an increasing MO-OOA mass during the day (red markers in Fig. 5b), similarly to the diurnal behaviour of sulphate (R^2=0.63). A night-time increase and a daytime decrease of the LO-OOA mass during spring and summer apparently followed condensation and re-evaporation cycles of semi-volatile species, similar to the behaviour of ammonium nitrate. Additionally, nocturnal chemistry of NO_3/N_2O_5 radicals could lead to formation of HNO_3 *via* N_2O_5 hydrolysis and of organic nitrates *via* oxidation of VOCs (Brown et al., 2004; Dentener and Crutzen, 1993), thus influencing the diurnal cycles of both particulate nitrate and LO-OOA (with R^2 = 0.48 for spring and R^2 = 0.36 for summer).

In Fig. 6, we also present the diurnal cycles of HOA, eBC_{tr} and NO_x with different patterns for weekdays and weekends. The hourly averages of HOA and eBC_{tr} as well as the NO_x mixing ratio peak during the morning and evening rush hours over the weekdays, while on the weekends there is only an evening pollution increase coinciding with the time when people come back from holidays or night-time leisure activities.

https://doi.org/10.5194/acp-2020-1263
Preprint. Discussion started: 22 December 2020

Atmospheric Chemistry and Physics Discussions

3.3.2 f_{44}/f_{43} analysis of secondary OA factors

While *m/z* 44 is mostly from the fragment of CO_2^+, a fingerprint of oxygenated species, *m/z* 43 can originate from $C_2H_3O^+$ (a fingerprint of semi-volatile species) or $C_3H_7^+$ (a fingerprint of the primary emissions of hydrocarbon-like species) (Canonaco et al., 2015; Duplissy et al., 2011; Ng et al., 2010). Thus, f_{44} and f_{43} are often used to identify the oxidation state of the factors, which is important to differentiate the MO-OOA and LO-OOA factors. Under the premise that the POA factors and the LOA factor are all well-resolved, it is important to investigate the relationship between the *m/z* 44 and *m/z* 43 signals in the OOA factors to determine whether or not one/two OOA factors are sufficient to explain the dataset. In addition, the shapes of the clouds shown in an f_{44} vs f_{43} plot may also include some source-related information. Figure 7 depicts the relationship between f_{44} and f_{43} of the two modelled OOA factors for different seasons. The yellow cloud of data points represents the measured f_{44} vs f_{43} after subtracting the *m/z* 44 and *m/z* 43 signals contributed by the primary HOA, BBOA and LOA factors. They are colour coded by the total OA mass concentration (data points with OA mass concentration below 2 $\mu g \cdot m^{-3}$ are hidden).

As shown in Fig. 7a, the data points in Sep–Oct (both in 2013 and 2014) were located on the right side of the triangle presented first by Ng et al. (2010), while the November (2013) data points were located within the triangle. In addition, the spring and summer data points (Fig. 7c and Fig. 7d) were all located rather on the right side of the triangle, but the winter points lied within the triangle (Fig. 7b). The data points located within the triangle correspond to the time with lower temperature than those are closer to the right side of the triangle (Fig. S9). This could be explained by the increased biogenic OOA emissions when the temperature was higher, as biogenic OOA tends to be distributed along the right side of the triangle (Canonaco et al., 2015; Pfaffenberger et al., 2013). Also, when the temperature decreases, the increased biomass

https://doi.org/10.5194/acp-2020-1263
Preprint. Discussion started: 22 December 2020


Atmospheric Chemistry and Physics Discussions

emissions make the OOA points to lie vertically within the triangle (Canonaco et al., 2015; Heringa et al., 2011), which is the case for the winter data (Fig. 7b).

In July 2014, the rolling PMF LO-OOA moved towards the left side of the plot due to increasing influences from *m/z* 80, *m/z* 94 ($C_2H_6S_2^+$), *m/z* 95, and *m/z* 96 (Fig. S7). Because the OA signal of *m/z* 80 is directly calculated from *m/z* 94 (Allan et al., 2004), we did not investigate the sources of *m/z* 80. A potential source of these distinct ions in July is dimethyl disulphide, which shows signals at *m/z* 94, *m/z* 95, and *m/z* 96 (NIST Mass Spectrometry Data Center, 2014). Dimethyl disulphide is widely used in pesticides. Considering that the sampling site is in the middle of farmland, and the diurnal variation of *m/z* 94 appeared to have peaks during the daytime, we considered the LO-OOA in July to be highly affected by the agricultural activities. However, the static factor profiles of summer LO-OOA from the seasonal summer solution had much smaller intensities for *m/z* 80 and *m/z* 94 (Fig. S6), which enhanced the scaled residuals for these two variables in the seasonal solutions.

In winter, LO-OOA (Fig. 9b) was highly affected by biomass burning emissions characterized by the presence of *m/z* 60, 73 (Alfarra et al., 2007), and the LO-OOA position in the f_{44} vs f_{43} space moved towards the right top direction in the plot due to the increasing biogenic influence as the temperature rose (Fig. 7b, Fig. S9) (Canonaco et al., 2015).

Figure 7 also highlights the advantages of rolling PMF over seasonal PMF due to its time-dependent source profiles. For all the seasons, both seasonal and rolling results show that the linear combinations of OOA factors could properly explain most of the measured OOA points. However, with the static OOA factors for seasonal PMF solutions, it remains difficult to capture the variabilities of some measured data points, while the rolling PMF OOA factors are able to move correspondingly with the temporal changes of the clouds, which moves the factor profiles closer to reality and potentially decreases the scaled residuals significantly (Fig. A3).

https://doi.org/10.5194/acp-2020-1263
Preprint. Discussion started: 22 December 2020


Atmospheric Chemistry and Physics Discussions

Figure S9 also shows the movements of LO-OOA and MO-OOA factor profiles monthly, where LO-OOA moves towards the right direction as the temperature increases, except for the two light blue squares (June and July) in Fig. S9a. It is clear that temperature plays an important role for the positions of LO-OOA and MO-OOA in the f_{44} vs f_{43} space due to its influences on the OOA sources (biogenic or anthropogenic) as well as the atmospheric processes, which is consistent with previous studies in Zurich (Canonaco et al., 2015).

3.3.3 Statistical and rotational uncertainties

As suggested by Canonaco et al. (2020), combining the bootstrap resampling and the random *a*-value techniques together with the rolling mechanism, we calculated the standard deviation (σ) and the mean (μ) of the mass concentration for each data point from each OA factor in selected "good" PMF runs. We estimated uncertainty of each OA factor using the slope of the linear fit of σ vs μ. (Fig. 8.). Since the LOA factor was tightly constrained with an *a*-value of 0.05, it has the smallest variability (4%). Overall, we found relatively smaller errors of HOA, BBOA, and MO-OOA (i.e., 18%, 14%, and 19%, respectively) and an error of 25% for LO-OOA which is comparable with the previous study (Canonaco et al., 2020). The errors for both the MO-OOA and the LO-OOA factor showed some temperature dependence. However, this actually varied with time, and the errors did not significantly change when we separated the dataset into four different temperature groups. Still, data points with higher temperature tend to have larger error for the total OOA than with lower temperature (Fig. 8f). This is because more complex aging processes for OOA factors at high temperature (>20 °C) can cause more variability for the OOA factors.

3.3.4 Online vs. offline

The mass concentrations for HOA, BBOA, and total OOA were compared with corresponding off-line AMS results (Vlachou et al., 2018) (Fig. S11). Despite some disagreement during

https://doi.org/10.5194/acp-2020-1263
Preprint. Discussion started: 22 December 2020


Atmospheric Chemistry and Physics Discussions

winter (BBOA and total OOA), BBOA showed a high correlation –with the offline results for both PM_{10} and $PM_{2.5}$, with R^2 of 0.83 and 0.84, respectively. The correlation for total OOA was somehow lower, with R^2 of 0.31 and 0.46 for the offline results of PM_{10} and $PM_{2.5}$ OOA, respectively. The enhanced OOA concentration for the rolling results during winter season compared to the offline SA results (Fig. 9a), as well as the differences between the rolling results and the offline $PM_{2.5}/PM_{10}$ results regarding BBOA are most likely due to the fact that the LO-OOA was heavily affected by biomass burning (Fig 9b). The offline results apportioned this biomass burning affected LO-OOA into BBOA, whereas the online ACSM measurements with a higher time resolution were capable to capture the fast oxidation process of biomass burning sources. In addition, the rolling PMF technique enabled the LO-OOA factor profile to adapt to the temporal viabilities of OA sources, so the relatively aged biomass burning related sources was apportioned into LO-OOA during winter time by rolling PMF. The yellow line in Fig. 9a depicts the mass concentration of *m/z* 60 within LO-OOA, which clearly shows significant enhancements during winter, as well as a good agreement with the LO-OOA time series. HOA did not correlate at all, which may be expected because HOA is not water soluble, and therefore has a very low recovery rate of 0.11 for the offline AMS technique based on the previous study by Daellenbach et al. (2016).

4 Conclusions

In this study, we conducted the first rolling PMF analysis on a 13-month ACSM data collected at a rural site of Switzerland. With the help of the a short rolling PMF time window together with the random *a*-value and bootstrap resampling analysis, we obtained a time dependent SA result with error estimations. Overall, we resolved a comprehensive 5-factor solution with HOA, BBOA, LOA, MO-OOA, and LO-OOA. The contribution of HOA was constant during the year (8.1–10.1%), while BBOA showed a clear seasonal variation (8.3–27.4%), which peaked during winter (due to an increased residential heating source) and contributed least in

https://doi.org/10.5194/acp-2020-1263
Preprint. Discussion started: 22 December 2020


Atmospheric Chemistry and Physics Discussions

summer. OOA was a dominant source throughout the year with a contribution of 71.6% on a yearly average. However, the biomass burning source had a strong influence on LO-OOA formation in winter. Together with BBOA, they make residential heating a considerable source at Magadino during winter. Therefore, a mitigation of residential wood combustion should be considered for a reduction of PM levels in Magadino, especially in winter.

This manuscript also provided a recommended criterion list (Table S1) as well as a novel way to define thresholds with minimum subjective judgements (student's *t*-test), which could be a leading example for other SoFi Pro users to conduct rolling PMF. To ensure a good representation of the modelled POA factors and to validate the SA results, we also used the correlations between the PMF factor time series and external data. Both HOA and BBOA agreed well with the corresponding external tracers (NO_x, eBC_{tr}, and eBC_{wb}) for the yearly cycles, except summer. This is because the aethalometer model for eBC SA has higher uncertainties with smaller eBC_{wb} mass concentrations. Also, NO_x could originate from multiple sources in this season. Therefore, we used HOA vs. eBC and $EV_{60,BBOA}$ to justify these two factors in summer. The correlation of HOA vs eBC had an R^2 of 0.28, with an $EV_{60,BBOA}$ of 0.55 in summer. Moreover, the MO-OOA and LO-OOA factors correlated well with inorganic SO_4 and NO_3, respectively. The identified primary and secondary OA factor profiles were consistent with the OA factors previously found at a variety of urban, rural, and remote European locations.

This paper assessed the statistical and rotational uncertainties of the PMF solution by combining the bootstrap resampling technique and the random *a*-value approach. It shows relatively small errors for constrained factors compared with a previous study in Zurich (Canonaco et al., 2020), and comparable errors for the OOA factors.

https://doi.org/10.5194/acp-2020-1263
Preprint. Discussion started: 22 December 2020

Atmospheric Chemistry and Physics Discussions

We also presented a head-to-head comparison between seasonal PMF solutions and the rolling PMF solution. The POA factors showed good agreement between seasonal and rolling PMF solution, while the OOA factors exhibited greater differences. Overall, the rolling PMF retrieved a somewhat better solution in terms of agreement with external tracers, but much better correlations between the OOA factors and corresponding inorganic salts. In addition, the rolling PMF results provided more realistic results by adapting the temporal variations of OOA factors in the f_{44} vs f_{43} space, which also led to much smaller scaled residuals than for the seasonal PMF. The time series of BBOA and total OOA agreed well with those from offline AMS AS results (Vlachou et al., 2018), except for winter when the fast oxidation processes of biomass burning emissions were not captured by the offline AMS technique.

Knowledge of diurnal, seasonal and annual changes in OA sources is essential for interpreting the yearly cycles of OA and defining mitigation strategies for air quality. With the help of more accurate and realistic OA sources together with an estimation of the statistical uncertainty of PMF more constraints can be provided both for climate and air quality models. These improved results are therefore highly valuable for policy makers to solve aerosol-related environmental issues.

5 Appendix A: Comparison between seasonal and rolling PMF solutions

The bootstrapped seasonal PMF solutions were compared with the full year rolling PMF results as follows. For each factor, the correlations with external data, the ion intensities in the factor profiles, and the mass concentrations retrieved from the two different source apportionment techniques were compared. The correlations of the factor time series with external data (i.e., NO_x, eBC_{tr}, eBC_{wb}, eBC_{totoal}, SO_4, NO_3, and NH_4) are presented in **Table A*1***. The rolling results showed generally slightly better correlations between LO-OOA and NO_3, MO-OOA

https://doi.org/10.5194/acp-2020-1263
Preprint. Discussion started: 22 December 2020

Atmospheric Chemistry and Physics Discussions

and SO_4, and total OOA with NH_4 than the seasonal PMF results, which is consistent with the comparison results from Canonaco et al. (2020). A significant improvement was evident for LO-OOA vs NO_3 in spring (with R^2 increasing from 0.02 to 0.48). Concerning the correlations of POA factors with external data, rolling results and seasonal showed similar results

Table A1 Correlation coefficients ($R^2_{pearson}$) between the factor contribution and expected tracers over the year and for individual meteorological seasons ($p<0.05$).

Factor	Yearly		SON_2013		DJF		MAM		JJA		SON_2014	
	Seasonal	Rolling	Seasonal	Rolling	Seasonal	Rolling	Seasonal	Rolling	Seasonal	Rolling	Seasonal	Rolling
HOA / NO_x	0.37	0.35	0.52	0.5	0.46	0.47	0.34	0.36	0.15	0.15	0.44	0.42
HOA / eBC_{tr}	0.34	0.33	0.29	0.35	0.41	0.42	0.39	0.31	N/A	N/A	0.38	0.39
HOA / eBC	0.55	0.51	0.79	0.77	0.77	0.73	0.5	0.41	0.29	0.28	0.5	0.47
BBOA / eBC_{wb}	0.82	0.82	0.81	0.79	0.84	0.81	0.67	0.6	N/A	N/A	0.3	0.27
MO-OOA / SO_4^{2-}	0.58	0.49	0.49	0.61	0.52	0.49	0.62	0.66	0.63	0.57	0.43	0.46
LO-OOA / NO_3^-	0.11	0.32	0.28	0.42	0.28	0.23	0.02	0.48	0.33	0.36	0.19	0.29
OOA/ NH_4^+	0.46	0.44	0.52	0.55	0.34	0.26	0.73	0.75	0.48	0.47	0.57	0.59

As shown in **Fig. A1** Comparison of the mass concentrations resulting from rolling PMF and from the seasonal analysis for each factor (colour coded by date and time)., which shows a good agreement for two techniques, except for MO-OOA and LO-OOA. In general, the slope of 1.09 for rolling total OOA vs seasonal OOA suggests a slight underestimation of the OOA contribution by the seasonal PMF solutions, while the slope (<1) for HOA and BBOA suggests that the seasonal PMF solutions overestimate HOA and BBOA. In addition, LOA shows the best agreement between the seasonal and rolling solutions, due to the tight constraint of LOA with an *a*-value of 0.05.

The LO-OOA and MO-OOA factors showed worse agreement than the POA factors for the whole dataset. They had good correlations in each meteorological season, however, with different slopes. For instance, seasonal PMF underestimated LO-OOA in spring and fall 2014, but both seasons showed high correlation with rather narrow scattering. The underestimation of LO-OOA by seasonal PMF was compensated by the overestimation of MO-OOA for these

https://doi.org/10.5194/acp-2020-1263
Preprint. Discussion started: 22 December 2020

Atmospheric Chemistry and Physics Discussions

two seasons, therefore, the summed OOA still showed a high correlation between rolling and seasonal PMF results. This is expected, as the rolling PMF allows the source profiles to adapt to temporal variations, while seasonal PMF only has static source profiles.

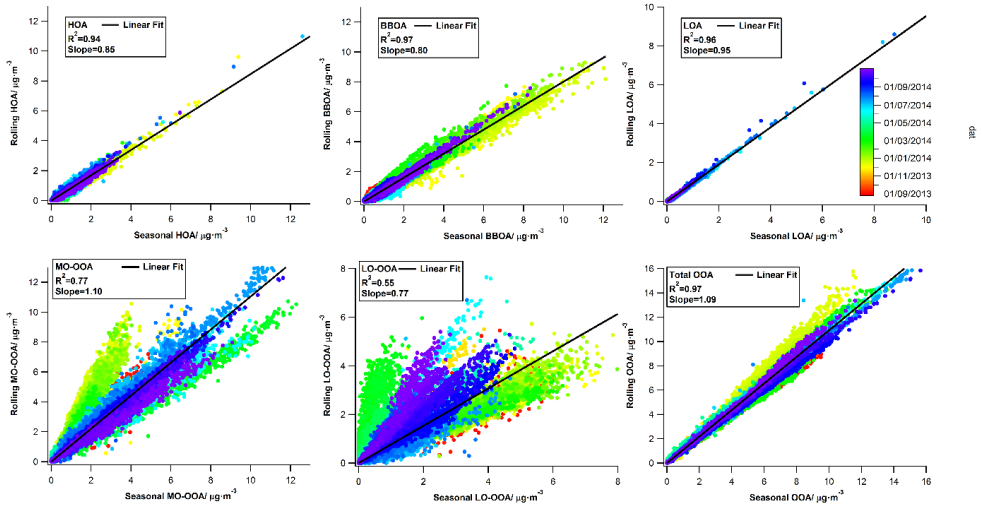

Fig. A1 Comparison of the mass concentrations resulting from rolling PMF and from the seasonal analysis for each factor (colour coded by date and time).

The differences in the major variables of the OOA factors (i.e., *m/z* 44, 43, and 60) shifted the mass concentrations significantly. Therefore, we also compared the factor profiles for both techniques (**Fig. A2**). For instance, LO-OOA during spring showed higher intensity at *m/z* 44 for the rolling PMF results than for the seasonal PMF results (**Fig. A2**), which caused the underestimation of LO-OOA for the seasonal PMF in spring. When we averaged the total OOA factor using mass-weighted MO-OOA and LO-OOA factors, rolling PMF yielded higher *m/z* 60 for all seasons. As a result, seasonal PMF slightly underestimated the summed OOA factors by around 9%, but slightly overestimated the POA factors by less than <6%.

https://doi.org/10.5194/acp-2020-1263
Preprint. Discussion started: 22 December 2020

Atmospheric Chemistry and Physics Discussions

632 The profiles of the constrained factors (HOA, BBOA, LOA) from the rolling results show very
633 high correlation with the seasonal results (**Fig. A2**), which suggests that the primary factors
634 and the tightly constrained factor (LOA) were consistent with the static profiles from the
635 seasonal PMF analysis.

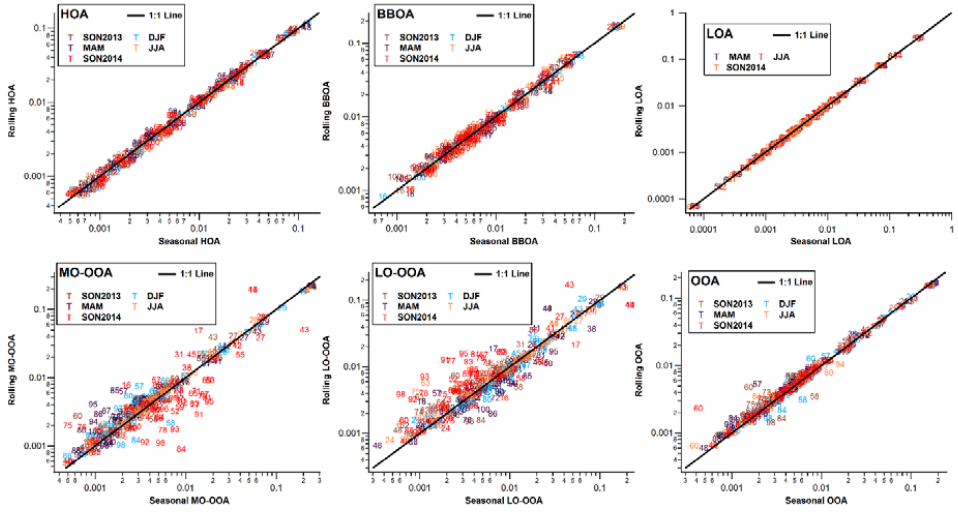

636

637 **Fig. A2** Profile comparisons between rolling results and seasonal results for each factor (log
638 scale).

639

640 We compared the scaled residuals from both source apportionment techniques (**Fig. A3**). The
641 rolling PMF solution had smaller scaled residuals (narrower histogram and the centre was
642 closer to 0) than that of the seasonal PMF solution, which is expected because rolling PMF had
643 more flexibility to adapt to the temporal variabilities of the OA sources.

https://doi.org/10.5194/acp-2020-1263
Preprint. Discussion started: 22 December 2020

Atmospheric Chemistry and Physics Discussions

644

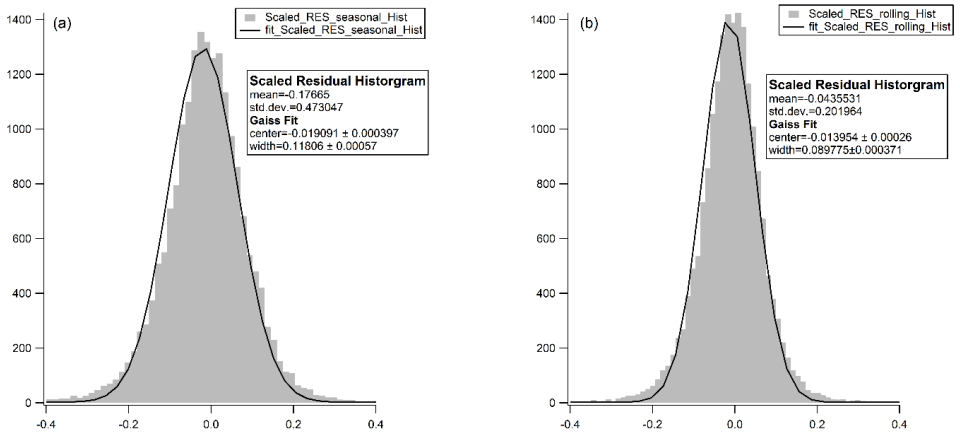

645

646 **Fig. A3** Distribution of the scaled residuals over the whole year for the seasonal solution (a)
647 and rolling solution (b).

648

649 Summarizing, HOA and BBOA were consistent for both rolling and seasonal PMF analysis in
650 terms of the time series, correlations with external tracers, and factor profiles due to the
651 consistency of their chemical factor profiles. In contrast, the MO-OOA and LO-OOA factors
652 were more scattered in terms of averaged factor profiles and mass concentration, which
653 suggests that seasonal PMF analysis was not sufficient to capture these temporal variabilities
654 of their oxidation processes. Also, rolling PMF showed smaller scaled residuals. Therefore, we
655 conclude that the rolling PMF analysis provides more realistic results than the seasonal analysis.

656 ## Data Availability

657 The data are available upon request to the corresponding author.

658 ## Competing interests

659 The authors declare no competing interests in any form for this work.

https://doi.org/10.5194/acp-2020-1263
Preprint. Discussion started: 22 December 2020

Atmospheric Chemistry and Physics Discussions

Author contributions

G. C. and Y. S. contributed equally for this manuscript. G. C. wrote the manuscript, illustrations as well as data treatments and processing. Y.S. wrote the preliminary manuscript and analysed preliminary results. R. F. and P. G. helped to run the campaign. P. G., and C. H. provided external data to validate PMF solution. F.C. provided technique support for SoFi Pro. F.C., A. T., K. R. D., A. V., J.G.S., I. EI. H., U. B., and A. S. H. P. participated discussions for this study.

Acknowledgements

The ACSM measurements were supported by the Swiss Federal Office for the Environment (FOEN). The leading role of the Environmental group of the Swiss Federal Laboratories for Materials and Testing (Empa) in supporting the measurements is very much appreciated. Y. S. acknowledges supports by the “Wiedereinsteigerinnen Program” at the Paul Scherrer Institute. This study was also supported by the cost action of Chemical On-Line cOmpoSition and Source Apportionment of fine aerosol (COLOSSAL, CA16109), a COST related project of the Swiss National Science Foundation, Source apportionment using long-term Aerosol Mass Spectrometry and Aethalometer Measurements (SAMSAM, IZCOZ0_177063), as well as the EU Horizon 2020 Framework Programme via the ERA-PLANET project SMURBS (grant agreement no. 689443).

References

Aiken, A. C., Salcedo, D., Cubison, M. J., Huffman, J. A., DeCarlo, P. F., Ulbrich, I. M., Docherty, K. S., Sueper, D., Kimmel, J. R., Worsnop, D. R., Trimborn, A., Northway, M., Stone, E. A., Schauer, J. J., Volkamer, R. M., Fortner, E., de Foy, B., Wang, J., Laskin, A., Shutthanandan, V., Zheng, J., Zhang, R., Gaffney, J., Marley, N. A., Paredes-Miranda, G.,

https://doi.org/10.5194/acp-2020-1263
Preprint. Discussion started: 22 December 2020


Atmospheric Chemistry and Physics Discussions

683 Arnott, W. P., Molina, L. T., Sosa, G. and Jimenez, J. L.: Mexico City aerosol analysis during
684 MILAGRO using high resolution aerosol mass spectrometry at the urban supersite (T0) – Part
685 1: Fine particle composition and organic source apportionment, Atmos. Chem. Phys., 9(17),
686 6633–6653, doi:10.5194/acp-9-6633-2009, 2009.

687 Alfarra, M. R., Prevot, A. S. H., Szidat, S., Sandradewi, J., Weimer, S., Lanz, V. A., Schreiber,
688 D., Mohr, M. and Baltensperger, U.: Identification of the Mass Spectral Signature of Organic
689 Aerosols from Wood Burning Emissions, Environ. Sci. Technol., 41(16), 5770–5777,
690 doi:10.1021/es062289b, 2007.

691 Allan, J. D., Alfarra, M. R., Bower, K. N., Williams, P. I., Gallagher, M. W., Jimenez, J. L.,
692 McDonald, A. G., Nemitz, E., Canagaratna, M. R., Jayne, J. T., Coe, H. and Worsnop, D. R.:
693 Quantitative sampling using an Aerodyne aerosol mass spectrometer 2. Measurements of fine
694 particulate chemical composition in two U.K. cities, J. Geophys. Res. Atmos., 108(D3), n/a-
695 n/a, doi:10.1029/2002JD002359, 2003.

696 Allan, J. D., Delia, A. E., Coe, H., Bower, K. N., Alfarra, M. R. R., Jimenez, J. L., Middlebrook,
697 A. M., Drewnick, F., Onasch, T. B., Canagaratna, M. R., Jayne, J. T. and Worsnop, D. R.: A
698 generalised method for the extraction of chemically resolved mass spectra from Aerodyne
699 aerosol mass spectrometer data, J. Aerosol Sci., 35(7), 909–922,
700 doi:10.1016/j.jaerosci.2004.02.007, 2004.

701 Bressi, M., Cavalli, F., Belis, C. A., Putaud, J.-P., Fröhlich, R., Martins dos Santos, S., Petralia,
702 E., Prévôt, A. S. H., Berico, M., Malaguti, A. and Canonaco, F.: Variations in the chemical
703 composition of the submicron aerosol and in the sources of the organic fraction at a regional
704 background site of the Po Valley (Italy), Atmos. Chem. Phys., 16(20), 12875–12896,
705 doi:10.5194/acp-16-12875-2016, 2016.

https://doi.org/10.5194/acp-2020-1263
Preprint. Discussion started: 22 December 2020

706 Brown, S. S., Dibb, J. E., Stark, H., Aldener, M., Vozella, M., Whitlow, S., Williams, E. J.,
707 Lerner, B. M., Jakoubek, R., Middlebrook, A. M., DeGouw, J. A., Warneke, C., Goldan, P. D.,
708 Kuster, W. C., Angevine, W. M., Sueper, D. T., Quinn, P. K., Bates, T. S., Meagher, J. F.,
709 Fehsenfeld, F. C. and Ravishankara, A. R.: Nighttime removal of NO x in the summer marine
710 boundary layer, Geophys. Res. Lett., 31(7), n/a-n/a, doi:10.1029/2004GL019412, 2004.

711 Canagaratna, M. R., Jayne, J. T., Jimenez, J. L., Allan, J. D., Alfarra, M. R., Zhang, Q., Onasch,
712 T. B., Drewnick, F., Coe, H., Middlebrook, A., Delia, A., Williams, L. R., Trimborn, A. M.,
713 Northway, M. J., DeCarlo, P. F., Kolb, C. E., Davidovits, P. and Worsnop, D. R.: Chemical
714 and microphysical characterization of ambient aerosols with the aerodyne aerosol mass
715 spectrometer, Mass Spectrom. Rev., 26(2), 185–222, doi:10.1002/mas.20115, 2007.

716 Canonaco, F., Crippa, M., Slowik, J. G., Baltensperger, U. and Prévôt, A. S. H. H.: SoFi, an
717 IGOR-based interface for the efficient use of the generalized multilinear engine (ME-2) for the
718 source apportionment: ME-2 application to aerosol mass spectrometer data, Atmos. Meas.
719 Tech., 6(12), 3649–3661, doi:10.5194/amt-6-3649-2013, 2013.

720 Canonaco, F., Slowik, J. G., Baltensperger, U. and Prévôt, A. S. H.: Seasonal differences in
721 oxygenated organic aerosol composition: implications for emissions sources and factor
722 analysis, Atmos. Chem. Phys., 15(12), 6993–7002, doi:10.5194/acp-15-6993-2015, 2015.

723 Canonaco, F., Tobler, A., Chen, G., Sosedova, Y., Slowik, J. G., Bozzetti, C., Daellenbach,
724 Kaspar Rudolf Haddad, I. El, Crippa, M., Huang, R.-J., Furger, M., Baltensperger, U. and
725 Prevot, A. S. H.: A new method for long-term source apportionment with time-dependent factor
726 profiles and uncertainty assessment using SoFi Pro: application to one year of organic aerosol
727 data, Atmos. Meas. Tech. Discuss., doi:10.5194/amt-2020-204, 2020.

728 Chow, J. C., Bachmann, J. D., Wierman, S. S. G., Mathai, C. V., Malm, W. C., White, W. H.,

https://doi.org/10.5194/acp-2020-1263
Preprint. Discussion started: 22 December 2020

729 Mueller, P. K., Kumar, N. and Watson, J. G.: Visibility: Science and Regulation, J. Air Waste
730 Manage. Assoc., 52(9), 973–999, doi:10.1080/10473289.2002.10470844, 2002.

731 Crippa, M., DeCarlo, P. F., Slowik, J. G., Mohr, C., Heringa, M. F., Chirico, R., Poulain, L.,
732 Freutel, F., Sciare, J., Cozic, J., Di Marco, C. F., Elsasser, M., Nicolas, J. B., Marchand, N.,
733 Abidi, E., Wiedensohler, A., Drewnick, F., Schneider, J., Borrmann, S., Nemitz, E.,
734 Zimmermann, R., Jaffrezo, J.-L., Prévôt, A. S. H. and Baltensperger, U.: Wintertime aerosol
735 chemical composition and source apportionment of the organic fraction in the metropolitan
736 area of Paris, Atmos. Chem. Phys., 13(2), 961–981, doi:10.5194/acp-13-961-2013, 2013.

737 Crippa, M., Canonaco, F., Lanz, V. A., Äijälä, M., Allan, J. D., Carbone, S., Capes, G.,
738 Ceburnis, D., Dall'Osto, M., Day, D. A., DeCarlo, P. F., Ehn, M., Eriksson, A.,
739 Freney, E., Hildebrandt Ruiz, L., Hillamo, R., Jimenez, J. L., Junninen, H., Kiendler-Scharr,
740 A., Kortelainen, A.-M., Kulmala, M., Laaksonen, A., Mensah, A. A., Mohr, C., Nemitz, E.,
741 O'Dowd, C., Ovadnevaite, J., Pandis, S. N., Petäjä, T., Poulain, L., Saarikoski, S.,
742 Sellegri, K., Swietlicki, E., Tiitta, P., Worsnop, D. R., Baltensperger, U. and Prévôt, A. S. H.
743 H.: Organic aerosol components derived from 25 AMS data sets across Europe using a
744 consistent ME-2 based source apportionment approach, Atmos. Chem. Phys., 14(12), 6159–
745 6176, doi:10.5194/acp-14-6159-2014, 2014.

746 Cubison, M. J., Ortega, A. M., Hayes, P. L., Farmer, D. K., Day, D., Lechner, M. J., Brune, W.
747 H., Apel, E., Diskin, G. S., Fisher, J. A., Fuelberg, H. E., Hecobian, A., Knapp, D. J., Mikoviny,
748 T., Riemer, D., Sachse, G. W., Sessions, W., Weber, R. J., Weinheimer, A. J., Wisthaler, A.
749 and Jimenez, J. L.: Effects of aging on organic aerosol from open biomass burning smoke in
750 aircraft and laboratory studies, Atmos. Chem. Phys., 11(23), 12049–12064, doi:www.atmos-
751 chem-phys.net/11/12049/2011/, 2011.

752 Daellenbach, K. R., Bozzetti, C., Křepelová, A., Canonaco, F., Wolf, R., Zotter, P., Fermo, P.,

https://doi.org/10.5194/acp-2020-1263
Preprint. Discussion started: 22 December 2020

753 Crippa, M., Slowik, J. G., Sosedova, Y., Zhang, Y., Huang, R.-J. J., Poulain, L., Szidat, S.,
754 Baltensperger, U., El Haddad, I. and Prévôt, A. S. H. H.: Characterization and source
755 apportionment of organic aerosol using offline aerosol mass spectrometry, Atmos. Meas. Tech.,
756 9(1), 23–39, doi:10.5194/amt-9-23-2016, 2016.

757 Daellenbach, K. R., Uzu, G., Jiang, J., Cassagnes, L.-E., Leni, Z., Vlachou, A., Stefenelli, G.,
758 Canonaco, F., Weber, S., Segers, A., Kuenen, J. J. P., Schaap, M., Favez, O., Albinet, A.,
759 Aksoyoglu, S., Dommen, J., Baltensperger, U., Geiser, M., El Haddad, I., Jaffrezo, J.-L. and
760 Prévôt, A. S. H.: Sources of particulate-matter air pollution and its oxidative potential in Europe,
761 Nature, 587(7834), 414–419, doi:10.1038/s41586-020-2902-8, 2020.

762 DeCarlo, P. F., Dunlea, E. J., Kimmel, J. R., Aiken, A. C., Sueper, D., Crounse, J., Wennberg,
763 P. O., Emmons, L., Shinozuka, Y., Clarke, A., Zhou, J., Tomlinson, J., Collins, D. R., Knapp,
764 D., Weinheimer, A. J., Montzka, D. D., Campos, T. and Jimenez, J. L.: Fast airborne aerosol
765 size and chemistry measurements above Mexico City and Central Mexico during the
766 MILAGRO campaign, Atmos. Chem. Phys., 8(14), 4027–4048, doi:10.5194/acp-8-4027-2008,
767 2008.

768 Dentener, F. J. and Crutzen, P. J.: Reaction of N 2 O 5 on tropospheric aerosols: Impact on the
769 global distributions of NO x , O 3 , and OH, J. Geophys. Res. Atmos., 98(D4), 7149–7163,
770 doi:10.1029/92JD02979, 1993.

771 Dockery, D. W. and Pope, C. A.: Acute Respiratory Effects of Particulate Air Pollution, Annu.
772 Rev. Public Health, 15(1), 107–132, doi:10.1146/annurev.pu.15.050194.000543, 1994.

773 Duplissy, J., DeCarlo, P. F., Dommen, J., Alfarra, M. R., Metzger, A., Barmpadimos, I., Prevot,
774 A. S. H., Weingartner, E., Tritscher, T., Gysel, M., Aiken, A. C., Jimenez, J. L., Canagaratna,
775 M. R., Worsnop, D. R., Collins, D. R., Tomlinson, J. and Baltensperger, U.: Relating

https://doi.org/10.5194/acp-2020-1263
Preprint. Discussion started: 22 December 2020


Atmospheric Chemistry and Physics Discussions

776 hygroscopicity and composition of organic aerosol particulate matter, Atmos. Chem. Phys.,
777 11(3), 1155–1165, doi:10.5194/acp-11-1155-2011, 2011.

778 Fröhlich, R., Cubison, M. J., Slowik, J. G., Bukowiecki, N., Prévôt, A. S. H. H., Baltensperger,
779 U., Schneider, J., Kimmel, J. R., Gonin, M., Rohner, U., Worsnop, D. R. and Jayne, J. T.: The
780 ToF-ACSM: a portable aerosol chemical speciation monitor with TOFMS detection, Atmos.
781 Meas. Tech., 6(11), 3225–3241, doi:10.5194/amt-6-3225-2013, 2013.

782 Fröhlich, R., Crenn, V., Setyan, A., Belis, C. A., Canonaco, F., Favez, O., Riffault, V., Slowik,
783 J. G., Aas, W., Aijälä, M., Alastuey, A., Artiñano, B., Bonnaire, N., Bozzetti, C., Bressi, M.,
784 Carbone, C., Coz, E., Croteau, P. L., Cubison, M. J., Esser-Gietl, J. K., Green, D. C., Gros, V.,
785 Heikkinen, L., Herrmann, H., Jayne, J. T., Lunder, C. R., Minguillón, M. C., Močnik, G.,
786 O'Dowd, C. D., Ovadnevaite, J., Petralia, E., Poulain, L., Priestman, M., Ripoll, A.,
787 Sarda-Estève, R., Wiedensohler, A., Baltensperger, U., Sciare, J. and Prévôt, A. S. H.: ACTRIS
788 ACSM intercomparison – Part 2: Intercomparison of ME-2 organic source apportionment
789 results from 15 individual, co-located aerosol mass spectrometers, Atmos. Meas. Tech., 8(6),
790 2555–2576, doi:10.5194/amt-8-2555-2015, 2015.

791 Heringa, M. F., DeCarlo, P. F., Chirico, R., Tritscher, T., Dommen, J., Weingartner, E., Richter,
792 R., Wehrle, G., Prévôt, A. S. H. and Baltensperger, U.: Investigations of primary and secondary
793 particulate matter of different wood combustion appliances with a high-resolution time-of-
794 flight aerosol mass spectrometer, Atmos. Chem. Phys., 11(12), 5945–5957, doi:10.5194/acp-
795 11-5945-2011, 2011.

796 Hildebrandt, L., Kostenidou, E., Lanz, V. A., Prevot, A. S. H. H., Baltensperger, U.,
797 Mihalopoulos, N., Laaksonen, A., Donahue, N. M. and Pandis, S. N.: Sources and atmospheric
798 processing of organic aerosol in the Mediterranean: insights from aerosol mass spectrometer
799 factor analysis, Atmos. Chem. Phys., 11(23), 12499–12515, doi:10.5194/acp-11-12499-2011,

https://doi.org/10.5194/acp-2020-1263
Preprint. Discussion started: 22 December 2020


Atmospheric Chemistry and Physics Discussions

800 2011.

801 Horvath, H.: Atmospheric light absorption—A review, Atmos. Environ. Part A. Gen. Top.,
802 27(3), 293–317, doi:10.1016/0960-1686(93)90104-7, 1993.

803 IPCC: Clouds and Aerosols, in Climate Change 2013 - The Physical Science Basis, edited by
804 Intergovernmental Panel on Climate Change, pp. 571–658, Cambridge University Press,
805 Cambridge., 2014.

806 Jacobson, M. C., Hansson, H.-C., Noone, K. J. and Charlson, R. J.: Organic atmospheric
807 aerosols: Review and state of the science, Rev. Geophys., 38(2), 267–294,
808 doi:10.1029/1998RG000045, 2000.

809 Jacobson, M. Z.: Global direct radiative forcing due to multicomponent anthropogenic and
810 natural aerosols, J. Geophys. Res. Atmos., 106(D2), 1551–1568, doi:10.1029/2000JD900514,
811 2001.

812 Jimenez, J. L., Canagaratna, M. R., Donahue, N. M., Prevot, A. S. H. H., Zhang, Q., Kroll, J.
813 H., DeCarlo, P. F., Allan, J. D., Coe, H., Ng, N. L., Aiken, A. C., Docherty, K. S., Ulbrich, I.
814 M., Grieshop, A. P., Robinson, A. L., Duplissy, J., Smith, J. D., Wilson, K. R., Lanz, V. A.,
815 Hueglin, C., Sun, Y. L., Tian, J., Laaksonen, A., Raatikainen, T., Rautiainen, J., Vaattovaara,
816 P., Ehn, M., Kulmala, M., Tomlinson, J. M., Collins, D. R., Cubison, M. J., Dunlea, J., Huffman,
817 J. A., Onasch, T. B., Alfarra, M. R., Williams, P. I., Bower, K., Kondo, Y., Schneider, J.,
818 Drewnick, F., Borrmann, S., Weimer, S., Demerjian, K., Salcedo, D., Cottrell, L., Griffin, R.,
819 Takami, A., Miyoshi, T., Hatakeyama, S., Shimono, A., Sun, J. Y., Zhang, Y. M., Dzepina, K.,
820 Kimmel, J. R., Sueper, D., Jayne, J. T., Herndon, S. C., Trimborn, A. M., Williams, L. R.,
821 Wood, E. C., Middlebrook, A. M., Kolb, C. E., Baltensperger, U., Worsnop, D. R., Dunlea, E.
822 J., Huffman, J. A., Onasch, T. B., Alfarra, M. R., Williams, P. I., Bower, K., Kondo, Y.,

https://doi.org/10.5194/acp-2020-1263
Preprint. Discussion started: 22 December 2020

823 Schneider, J., Drewnick, F., Borrmann, S., Weimer, S., Demerjian, K., Salcedo, D., Cottrell,
824 L., Griffin, R., Takami, A., Miyoshi, T., Hatakeyama, S., Shimono, A., Sun, J. Y., Zhang, Y.
825 M., Dzepina, K., Kimmel, J. R., Sueper, D., Jayne, J. T., Herndon, S. C., Trimborn, A. M.,
826 Williams, L. R., Wood, E. C., Middlebrook, A. M., Kolb, C. E., Baltensperger, U. and Worsnop,
827 D. R.: Evolution of Organic Aerosols in the Atmosphere, Science (80-.)., 326(5959), 1525–
828 1529, doi:10.1126/science.1180353, 2009.

829 Lanz, V. A., Alfarra, M. R., Baltensperger, U., Buchmann, B., Hueglin, C. and Prévôt, A. S.
830 H.: Source apportionment of submicron organic aerosols at an urban site by factor analytical
831 modelling of aerosol mass spectra, Atmos. Chem. Phys., 7(6), 1503–1522, doi:10.5194/acp-7-
832 1503-2007, 2007.

833 Lanz, V. A., Alfarra, M. R., Baltensperger, U., Buchmann, B., Hueglin, C., Szidat, S., Wehrli,
834 M. N., Wacker, L., Weimer, S., Caseiro, A., Puxbaum, H. and Prevot, A. S. H.: Source
835 Attribution of Submicron Organic Aerosols during Wintertime Inversions by Advanced Factor
836 Analysis of Aerosol Mass Spectra, Environ. Sci. Technol., 42(1), 214–220,
837 doi:10.1021/es0707207, 2008.

838 Lelieveld, J., Evans, J. S., Fnais, M., Giannadaki, D. and Pozzer, A.: The contribution of
839 outdoor air pollution sources to premature mortality on a global scale, Nature, 525(7569), 367–
840 371, doi:10.1038/nature15371, 2015.

841 Matthew, B. M., Middlebrook, A. M. and Onasch, T. B.: Collection Efficiencies in an
842 Aerodyne Aerosol Mass Spectrometer as a Function of Particle Phase for Laboratory Generated
843 Aerosols, Aerosol Sci. Technol., 42(11), 884–898, doi:10.1080/02786820802356797, 2008.

844 Mauderly, J. L. and Chow, J. C.: Health Effects of Organic Aerosols, Inhal. Toxicol., 20(3),
845 257–288, doi:10.1080/08958370701866008, 2008.

https://doi.org/10.5194/acp-2020-1263
Preprint. Discussion started: 22 December 2020


Atmospheric Chemistry and Physics Discussions

846 Meteotest: Data Report Switzerland 2007 – 2016, Bern, Switzerland., 2017.

847 Middlebrook, A. M., Bahreini, R., Jimenez, J. L. and Canagaratna, M. R.: Evaluation of
848 Composition-Dependent Collection Efficiencies for the Aerodyne Aerosol Mass Spectrometer
849 using Field Data, Aerosol Sci. Technol., 46(3), 258–271, doi:10.1080/02786826.2011.620041,
850 2012.

851 Minguillón, M. C., Ripoll, A., Pérez, N., Prévôt, A. S. H., Canonaco, F., Querol, X. and
852 Alastuey, A.: Chemical characterization of submicron regional background aerosols in the
853 western Mediterranean using an Aerosol Chemical Speciation Monitor, Atmos. Chem. Phys.,
854 15(11), 6379–6391, doi:10.5194/acp-15-6379-2015, 2015.

855 Mohr, C., Decarlo, P. F., Heringa, M. F., Chirico, R., Slowik, J. G., Richter, R., Reche, C.,
856 Alastuey, A., Querol, X., Seco, R., Crippa, M., Zimmermann, R., Baltensperger, U., Barcelona,
857 D., Munchen, H. Z. and Mass, J.: Wintertime aerosol chemical composition and source
858 apportionment of the organic fraction in the metropolitan area of Paris, Atmos. Chem. Phys.,
859 12(4), 1649–1665, doi:10.5194/acp-13-961-2013, 2012.

860 Monn, C.: Exposure assessment of air pollutants: a review on spatial heterogeneity and
861 indoor/outdoor/personal exposure to suspended particulate matter, nitrogen dioxide and ozone,
862 Atmos. Environ., 35(1), 1–32, doi:10.1016/S1352-2310(00)00330-7, 2001.

863 Murphy, D. M., Cziczo, D. J., Froyd, K. D., Hudson, P. K., Matthew, B. M., Middlebrook, A.
864 M., Peltier, R. E., Sullivan, A., Thomson, D. S. and Weber, R. J.: Single-particle mass
865 spectrometry of tropospheric aerosol particles, J. Geophys. Res. Atmos., 111(D23), n/a-n/a,
866 doi:10.1029/2006JD007340, 2006.

867 Ng, N. L., Canagaratna, M. R., Zhang, Q., Jimenez, J. L., Tian, J., Ulbrich, I. M., Kroll, J. H.,
868 Docherty, K. S., Chhabra, P. S., Bahreini, R., Murphy, S. M., Seinfeld, J. H., Hildebrandt, L.,

https://doi.org/10.5194/acp-2020-1263
Preprint. Discussion started: 22 December 2020

869 Donahue, N. M., DeCarlo, P. F., Lanz, V. A., Prévôt, A. S. H. H., Dinar, E., Rudich, Y. and
870 Worsnop, D. R.: Organic aerosol components observed in Northern Hemispheric datasets from
871 Aerosol Mass Spectrometry, Atmos. Chem. Phys., 10(10), 4625–4641, doi:10.5194/acp-10-
872 4625-2010, 2010.

873 Ng, N. L., Herndon, S. C., Trimborn, A., Canagaratna, M. R., Croteau, P. L., Onasch, T. B.,
874 Sueper, D., Worsnop, D. R., Zhang, Q., Sun, Y. L. and Jayne, J. T.: An Aerosol Chemical
875 Speciation Monitor (ACSM) for Routine Monitoring of the Composition and Mass
876 Concentrations of Ambient Aerosol, Aerosol Sci. Technol., 45(7), 780–794,
877 doi:10.1080/02786826.2011.560211, 2011a.

878 Ng, N. L., Canagaratna, M. R., Jimenez, J. L., Zhang, Q., Ulbrich, I. M. and Worsnop, D. R.:
879 Real-Time Methods for Estimating Organic Component Mass Concentrations from Aerosol
880 Mass Spectrometer Data, Environ. Sci. Technol., 45(3), 910–916, doi:10.1021/es102951k,
881 2011b.

882 NIST Mass Spectrometry Data Center: Disulfide, dimethyl, SRD 69. [online] Available from:
883 https://webbook.nist.gov/cgi/cbook.cgi?ID=C624920&Mask=200#Refs (Accessed 6 August
884 2020), 2014.

885 Paatero, P.: The Multilinear Engine—A Table-Driven, Least Squares Program for Solving
886 Multilinear Problems, Including the n -Way Parallel Factor Analysis Model, J. Comput. Graph.
887 Stat., 8(4), 854–888, doi:10.1080/10618600.1999.10474853, 1999.

888 Paatero, P. and Hopke, P. K.: Discarding or downweighting high-noise variables in factor
889 analytic models, Anal. Chim. Acta, 490(1–2), 277–289, doi:10.1016/S0003-2670(02)01643-4,
890 2003.

891 Paatero, P. and Hopke, P. K.: Rotational tools for factor analytic models, J. Chemom., 23(2),

https://doi.org/10.5194/acp-2020-1263
Preprint. Discussion started: 22 December 2020

892 91–100, doi:10.1002/cem.1197, 2009.

893 Paatero, P. and Tapper, U.: Positive matrix factorization: A non-negative factor model with
894 optimal utilization of error estimates of data values, Environmetrics, 5(2), 111–126,
895 doi:10.1002/env.3170050203, 1994.

896 Paatero, P., Eberly, S., Brown, S. G. and Norris, G. A.: Methods for estimating uncertainty in
897 factor analytic solutions, Atmos. Meas. Tech., 7(3), 781–797, doi:10.5194/amt-7-781-2014,
898 2014.

899 Parworth, C., Fast, J., Mei, F., Shippert, T., Sivaraman, C., Tilp, A., Watson, T. and Zhang, Q.:
900 Long-term measurements of submicrometer aerosol chemistry at the Southern Great Plains
901 (SGP) using an Aerosol Chemical Speciation Monitor (ACSM), Atmos. Environ., 106, 43–55,
902 doi:10.1016/j.atmosenv.2015.01.060, 2015.

903 Petit, J.-E., Favez, O., Sciare, J., Canonaco, F., Croteau, P., Močnik, G., Jayne, J., Worsnop, D.
904 and Leoz-Garziandia, E.: Submicron aerosol source apportionment of wintertime pollution in
905 Paris, France by double positive matrix factorization
906 (PMF²) using an aerosol chemical speciation
907 monitor (ACSM) and a multi-wavelength Aethalometer, Atmos. Chem. Phys., 14(24), 13773–
908 13787, doi:10.5194/acp-14-13773-2014, 2014.

909 Pfaffenberger, L., Barmet, P., Slowik, J. G., Praplan, A. P., Dommen, J., Prévôt, A. S. H. and
910 Baltensperger, U.: The link between organic aerosol mass loading and degree of oxygenation:
911 an α-pinene photooxidation study, Atmos. Chem. Phys., 13(13), 6493–6506, doi:10.5194/acp-
912 13-6493-2013, 2013.

913 Pope, C. A. and Dockery, D. W.: Health Effects of Fine Particulate Air Pollution: Lines that
914 Connect, J. Air Waste Manage. Assoc., 56(6), 709–742,

915 doi:10.1080/10473289.2006.10464485, 2006.

916 Ramanathan, V., Chung, C., Kim, D., Bettge, T., Buja, L., Kiehl, J. T., Washington, W. M., Fu,
917 Q., Sikka, D. R. and Wild, M.: Atmospheric brown clouds: Impacts on South Asian climate
918 and hydrological cycle, Proc. Natl. Acad. Sci., 102(15), 5326–5333,
919 doi:10.1073/pnas.0500656102, 2005.

920 Reyes-Villegas, E., Green, D. C., Priestman, M., Canonaco, F., Coe, H., Prévôt, A. S. H. and
921 Allan, J. D.: Organic Aerosol source apportionment in London 2013 with ME-2: exploring the
922 solution space with annual and seasonal analysis, Atmos. Chem. Phys. Discuss., 1–18,
923 doi:10.5194/acp-2016-465, 2016.

924 Ripoll, A., Minguillón, M. C., Pey, J., Jimenez, J. L., Day, D. A., Sosedova, Y., Canonaco, F.,
925 Prévôt, A. S. H., Querol, X. and Alastuey, A.: Long-term real-time chemical characterization
926 of submicron aerosols at Montsec (southern Pyrenees, 1570 m a.s.l.), Atmos. Chem. Phys.,
927 15(6), 2935–2951, doi:10.5194/acp-15-2935-2015, 2015.

928 von Schneidemesser, E., Monks, P. S., Allan, J. D., Bruhwiler, L., Forster, P., Fowler, D., Lauer,
929 A., Morgan, W. T., Paasonen, P., Righi, M., Sindelarova, K. and Sutton, M. A.: Chemistry and
930 the Linkages between Air Quality and Climate Change, Chem. Rev., 115(10), 3856–3897,
931 doi:10.1021/acs.chemrev.5b00089, 2015.

932 Schurman, M. I., Lee, T., Sun, Y., Schichtel, B. A., Kreidenweis, S. M. and Collett Jr., J. L.:
933 Investigating types and sources of organic aerosol in Rocky Mountain National Park using
934 aerosol mass spectrometry, Atmos. Chem. Phys., 15(2), 737–752, doi:10.5194/acp-15-737-
935 2015, 2015.

936 Schwarz, J. P., Gao, R. S., Perring, A. E., Spackman, J. R. and Fahey, D. W.: Black carbon
937 aerosol size in snow, Sci. Rep., 3, 1–5, doi:10.1038/srep01356, 2013.

https://doi.org/10.5194/acp-2020-1263
Preprint. Discussion started: 22 December 2020


Atmospheric Chemistry and Physics Discussions

938 Sug Park, E., Henry, R. C. and Spiegelman, C. H.: Estimating the number of factors to include
939 in a high-dimensional multivariate bilinear model, Commun. Stat. - Simul. Comput., 29(3),
940 723–746, doi:10.1080/03610910008813637, 2000.

941 Szidat, S., Prévôt, A. S. H., Sandradewi, J., Alfarra, M. R., Synal, H.-A., Wacker, L. and
942 Baltensperger, U.: Dominant impact of residential wood burning on particulate matter in
943 Alpine valleys during winter, Geophys. Res. Lett., 34(5), doi:10.1029/2006GL028325, 2007.

944 The Swiss Federal Council: Ordinance of 16 December 1985 on Air Pollution Control (OAPC).
945 [online] Available from: https://www.admin.ch/opc/en/classified-
946 compilation/19850321/index.html#app7 (Accessed 10 September 2019), 2018.

947 Tobler, A., Bhattu, D., Canonaco, F., Lalchandani, V., Shukla, A., Thamban, N. M., Mishra,
948 S., Srivastava, A. K., Bisht, D. S., Tiwari, S., Singh, S., Močnik, G., Baltensperger, U., Tripathi,
949 S. N., Slowik, J. G. and Prévôt, A. S. H.: Chemical characterization of PM2.5 and source
950 apportionment of organic aerosol in New Delhi, India, Sci. Total Environ., 745, 1–12,
951 doi:10.1016/j.scitotenv.2020.140924, 2020.

952 Ulbrich, I. M., Canagaratna, M. R., Zhang, Q., Worsnop, D. R. and Jimenez, J. L.:
953 Interpretation of organic components from Positive Matrix Factorization of aerosol mass
954 spectrometric data, Atmos. Chem. Phys., 9(9), 2891–2918, doi:10.5194/acp-9-2891-2009,
955 2009.

956 Vlachou, A., Daellenbach, K. R., Bozzetti, C., Chazeau, B., Salazar, G. A., Szidat, S., Jaffrezo,
957 J.-L., Hueglin, C., Baltensperger, U., Haddad, I. El and Prévôt, A. S. H.: Advanced source
958 apportionment of carbonaceous aerosols by coupling offline AMS and radiocarbon size-
959 segregated measurements over a nearly 2-year period, Atmos. Chem. Phys., 18(9), 6187–6206,
960 doi:10.5194/acp-18-6187-2018, 2018.

https://doi.org/10.5194/acp-2020-1263
Preprint. Discussion started: 22 December 2020

961 Zhang, Q., Jimenez, J. L., Canagaratna, M. R., Allan, J. D., Coe, H., Ulbrich, I., Alfarra, M. R.,
962 Takami, A., Middlebrook, A. M., Sun, Y. L., Dzepina, K., Dunlea, E., Docherty, K., DeCarlo,
963 P. F., Salcedo, D., Onasch, T., Jayne, J. T., Miyoshi, T., Shimono, A., Hatakeyama, S.,
964 Takegawa, N., Kondo, Y., Schneider, J., Drewnick, F., Borrmann, S., Weimer, S., Demerjian,
965 K., Williams, P., Bower, K., Bahreini, R., Cottrell, L., Griffin, R. J., Rautiainen, J., Sun, J. Y.,
966 Zhang, Y. M. and Worsnop, D. R.: Ubiquity and dominance of oxygenated species in organic
967 aerosols in anthropogenically-influenced Northern Hemisphere midlatitudes, Geophys. Res.
968 Lett., 34(13), n/a-n/a, doi:10.1029/2007GL029979, 2007.

969 Zhang, Q., Jimenez, J. L., Canagaratna, M. R., Ulbrich, I. M., Ng, N. L., Worsnop, D. R. and
970 Sun, Y.: Understanding atmospheric organic aerosols via factor analysis of aerosol mass
971 spectrometry: a review, Anal. Bioanal. Chem., 401(10), 3045–3067, doi:10.1007/s00216-011-
972 5355-y, 2011.

973 Zhang, Y., Favez, O., Petit, J.-E., Canonaco, F., Truong, F., Bonnaire, N., Crenn, V., Amodeo,
974 T., Prévôt, A. S. H., Sciare, J., Gros, V. and Albinet, A.: Six-year source apportionment of
975 submicron organic aerosols from near-continuous highly time-resolved measurements at
976 SIRTA (Paris area, France), Atmos. Chem. Phys., 19(23), 14755–14776, doi:10.5194/acp-19-
977 14755-2019, 2019.

978 Zotter, P., Herich, H., Gysel, M., El-Haddad, I., Zhang, Y., Močnik, G., Hüglin, C.,
979 Baltensperger, U., Szidat, S. and Prévôt, A. S. H.: Evaluation of the absorption Ångström
980 exponents for traffic and wood burning in the Aethalometer-based source apportionment using
981 radiocarbon measurements of ambient aerosol, Atmos. Chem. Phys., 17(6), 4229–4249,
982 doi:10.5194/acp-17-4229-2017, 2017.

983

https://doi.org/10.5194/acp-2020-1263
Preprint. Discussion started: 22 December 2020

Atmospheric Chemistry and Physics Discussions

984

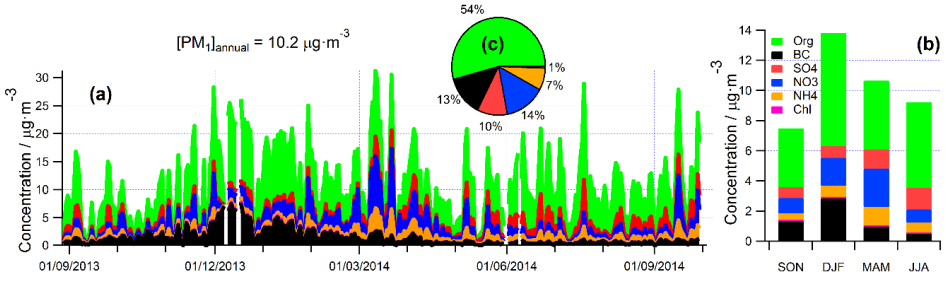

985

986 **Fig. 1** Chemical composition of PM_1 in Magadino 2013-2014 – daily (a), seasonal (b) and
987 annual (c) averages. The labels indicate the non-refractory organics (Org), sulphate (SO_4),
988 nitrate (NO_3), ammonium (NH_4) and chloride (Cl) ions measured by ACSM, and the black
989 carbon (BC) measured by light absorption.

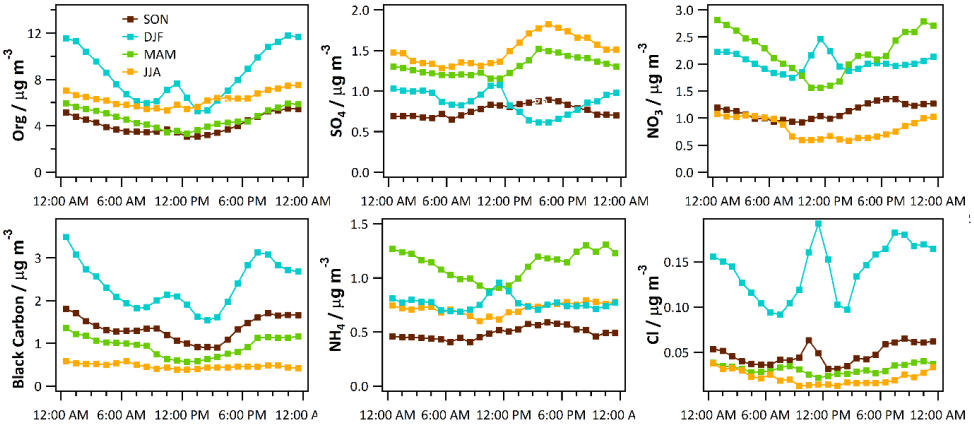

990

991 **Fig. 2** Seasonal diurnal cycles of PM_1 constituents calculated as an hourly average for ACSM
992 organic and inorganic species (sulphate, nitrate, ammonium, and chloride) and black carbon

https://doi.org/10.5194/acp-2020-1263
Preprint. Discussion started: 22 December 2020

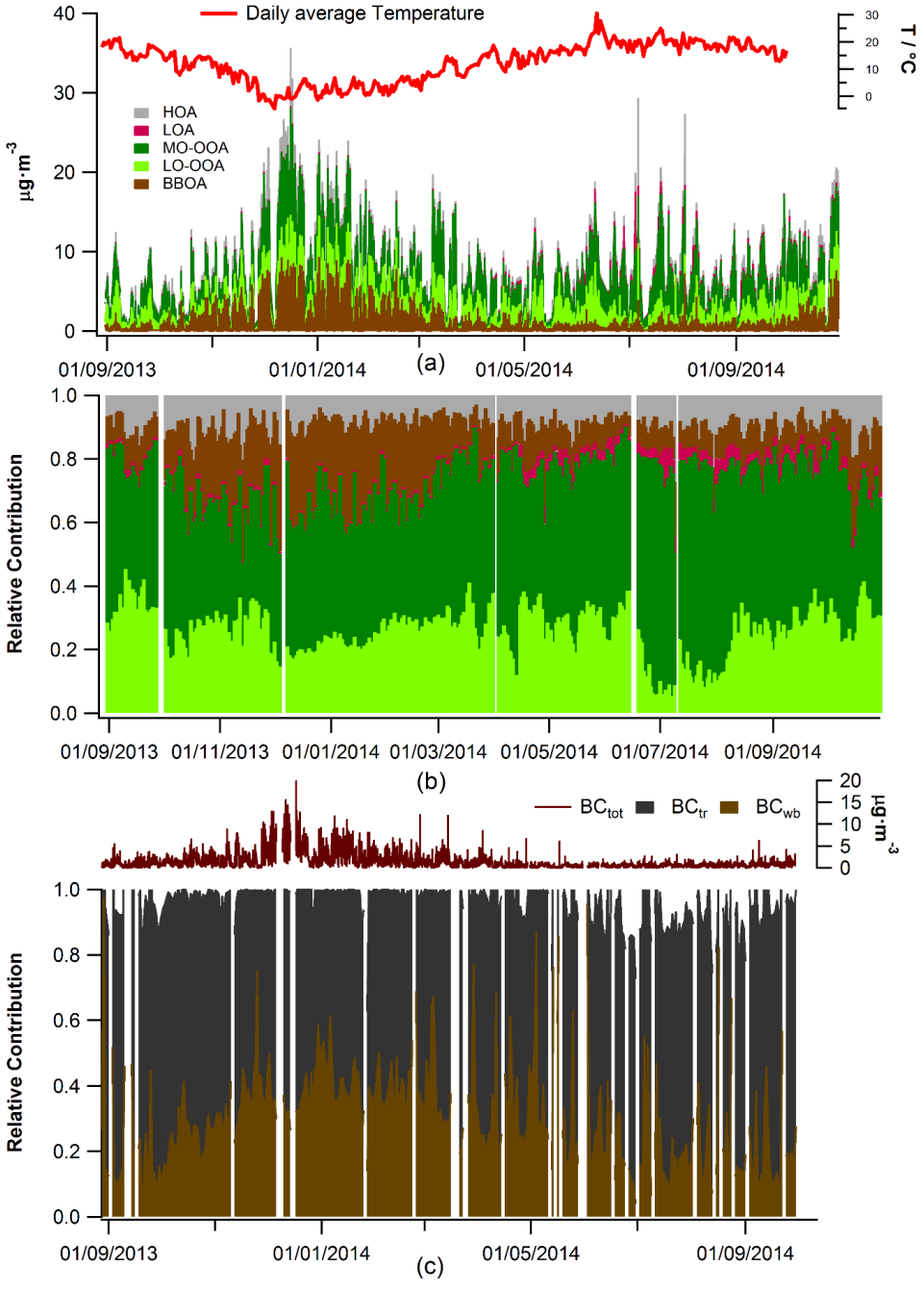

993

994 **Fig. 3** Annual cycle of OA sources: (a) absolute and (b) relative OA contributions plotted as

995 30-min resolved time series, (c) BC source apportionment.

https://doi.org/10.5194/acp-2020-1263
Preprint. Discussion started: 22 December 2020

Atmospheric Chemistry and Physics Discussions

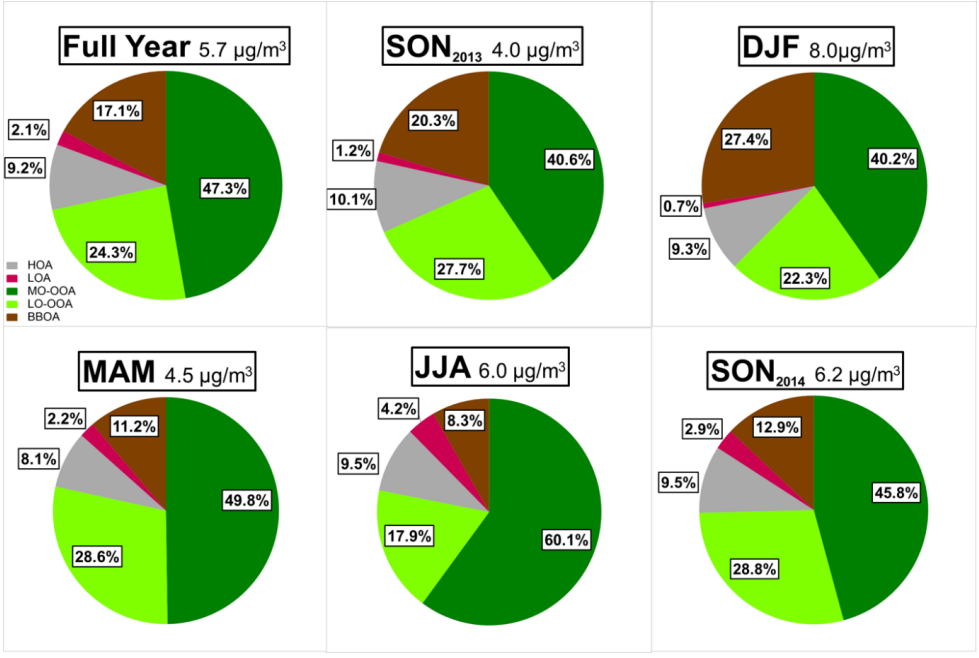

996

997 **Fig. 4** OA pie charts for the whole year and for different seasons.

https://doi.org/10.5194/acp-2020-1263
Preprint. Discussion started: 22 December 2020

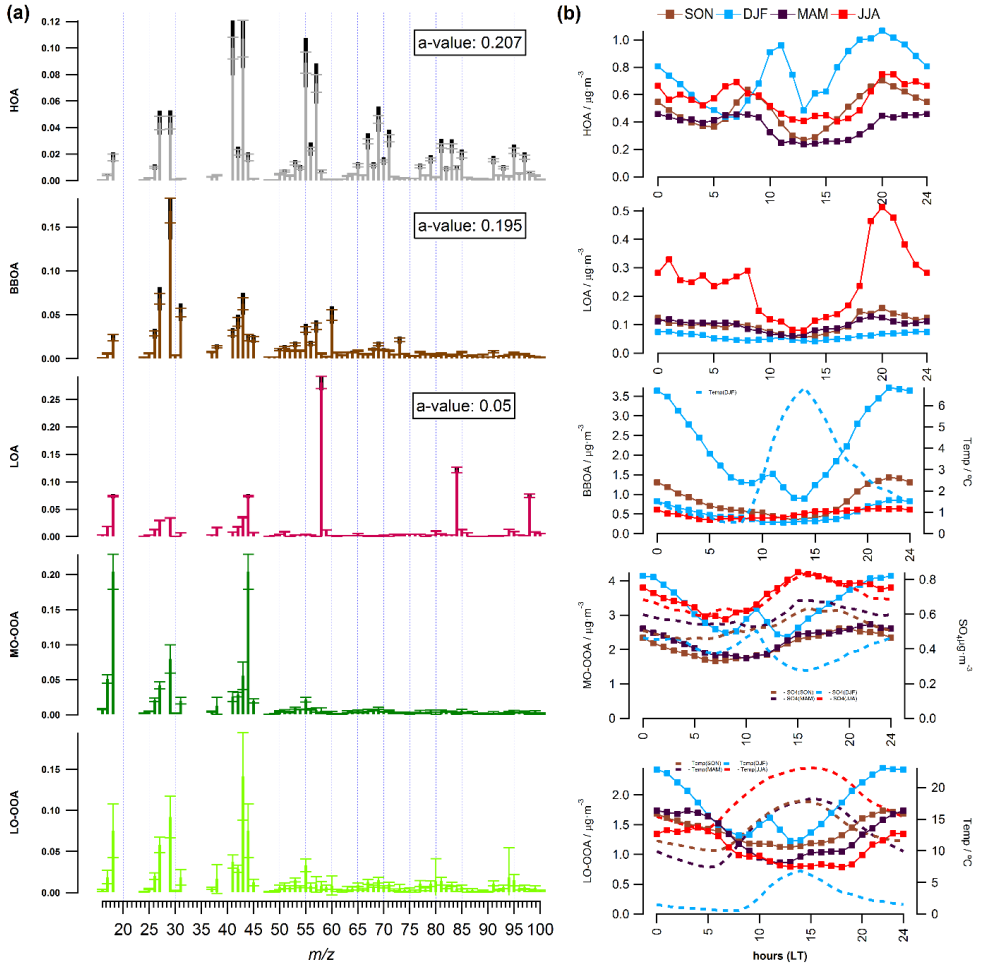

998

999 **Fig. 5** Overview of the primary and secondary OA sources in Magadino in 2013-2014: (a) OA
1000 factor profiles and (b) seasonal diurnal cycles of HOA, BBOA, LOA, MO-OOA, and LO-
1001 OOA. The ambient temperature is shown on the LO-OOA diurnal plots, respectively. In (a) the
1002 error bar is the standard deviation; the black bars show the maximum and the minimum that
1003 the variable allowed to be vary from the reference profiles. The average, 10th and 90th
1004 percentiles for a-values of HOA are, 0.195, 0.007 and 0.378, respectively. Also, the average,
1005 10th and 90th percentiles for a-values of BBOA are 0.202, 0.025 and 0.379, respectively.

https://doi.org/10.5194/acp-2020-1263
Preprint. Discussion started: 22 December 2020

Atmospheric Chemistry and Physics Discussions

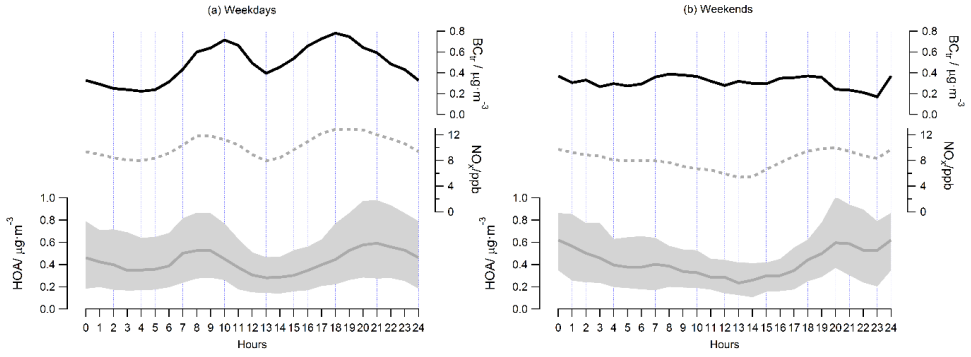

Fig. 6 Diurnal cycles of HOA (grey symbols), black carbon apportioned to traffic emissions eBC$_{tr}$ (dashed lines) and NO$_x$ (dotted lines) for weekdays (a) and weekends (b). The shaded areas represent interquartile range for 1-hour average HOA.

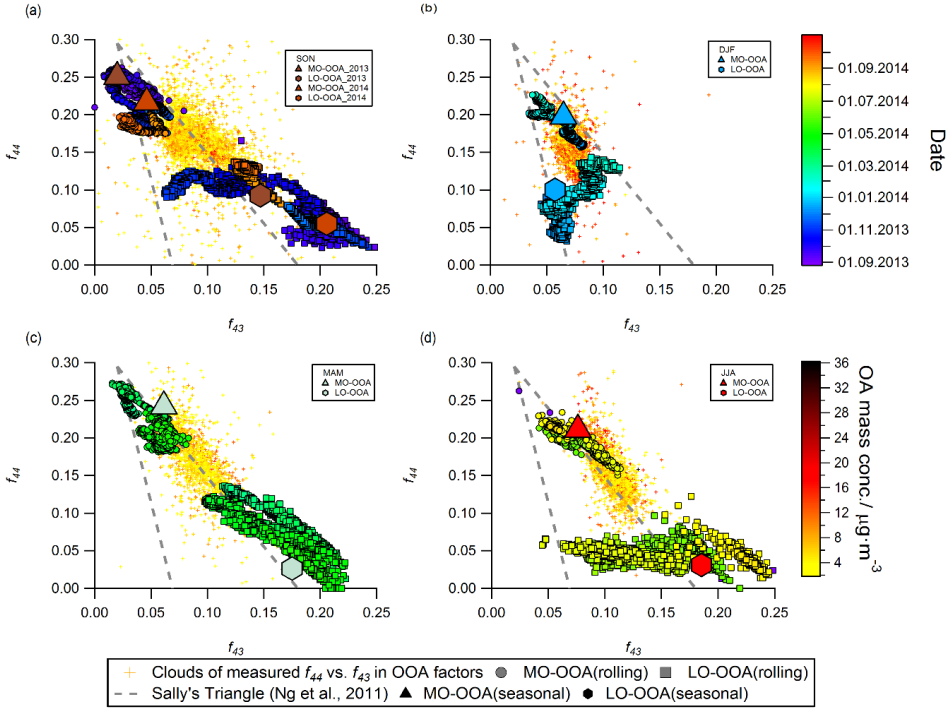

Fig. 7 OOA f_{44} and f_{43} for four different seasons. The yellow cloud of data points represents the f_{44} vs f_{43} by subtracting the f_{44} and f_{43} contributed from HOA, BBOA and LOA factors. They are color coded by the total OA mass concentration. The circles, triangles, and squares

https://doi.org/10.5194/acp-2020-1263
Preprint. Discussion started: 22 December 2020


Atmospheric Chemistry and Physics Discussions

represent the ratio between f_{44} and f_{43} intensities within the factor profiles of MO-OOA and LO-OOA, respectively. While the smaller size of circles, triangles, and squares are from rolling PMF analysis, which are color coded by the date and time. The dash line are the Sally's triangle from (Ng et al., 2011) and depicts the region where several PMF OOA from the last decade resided in the f_{44} vs f_{43} space.

https://doi.org/10.5194/acp-2020-1263
Preprint. Discussion started: 22 December 2020

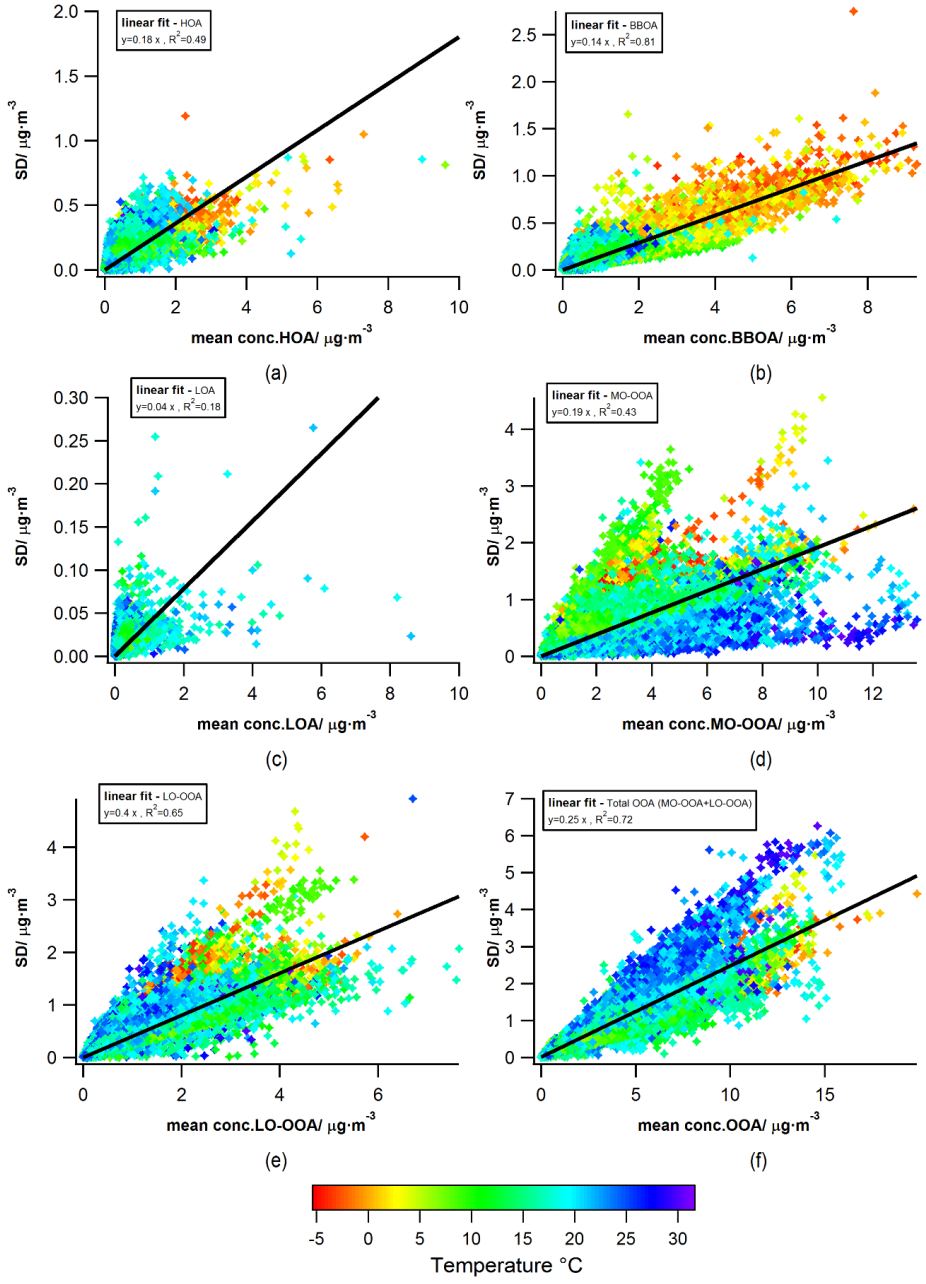

1019

1020 **Fig. 8** Absolute statistical uncertainties of PMF for HOA, BBOA, LOA, LO-OOA, MO-OOA

1021 and total OOA (LO-OOA+MO-OOA) for all data. The data points colour-coded all data points

https://doi.org/10.5194/acp-2020-1263
Preprint. Discussion started: 22 December 2020

Atmospheric Chemistry and Physics Discussions

1022 by temperature. The PMF error (uncertainties) of selected PMF runs and rotational
1023 uncertainties is estimated using the slope of the linear regression of standard deviation (σ) vs.
1024 the averaged mass concentration (μ) for each factor.

1025

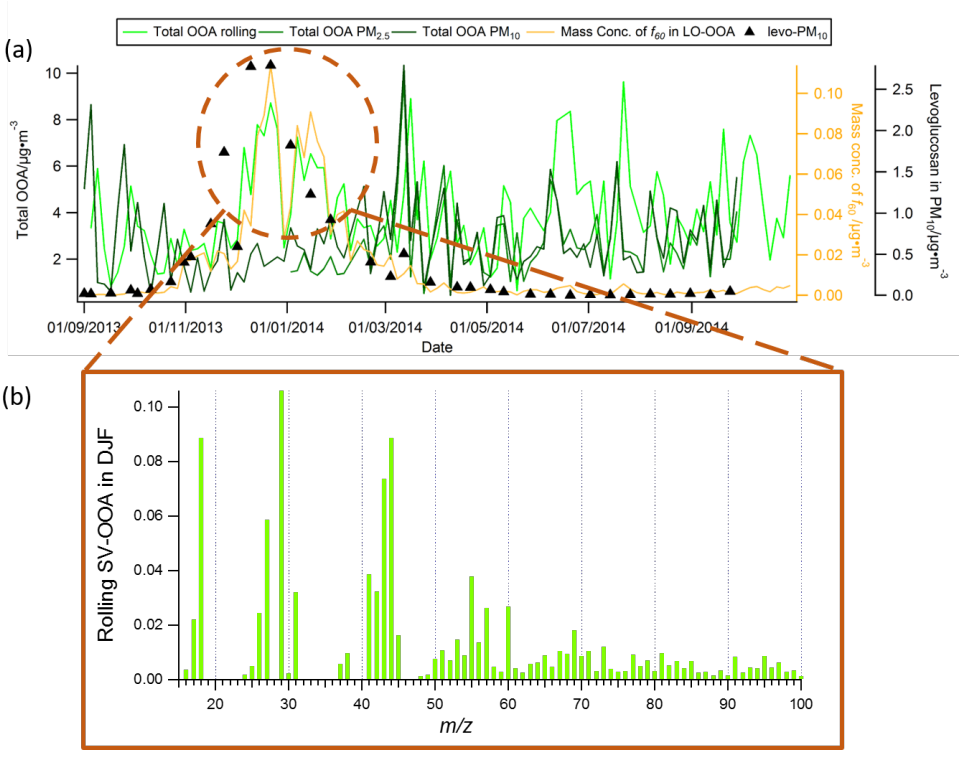

1026

1027 **Fig. 9** (a) Time series of total oxygenated organic aerosol (LO-OOA+MO-OOA) from online
1028 and offline source apportionment solutions, together with f60 in LO-OOA for online solution,
1029 and levoglucosan in PM10 filter; (b) Averaged LO-OOA factor profile from online solution
1030 during DJF (Dec, Jan, and Feb), when online total OOA is significantly higher than that of
1031 offline solutions.